REPORT DOCUMENTATION PAGE

Form Approved
OMB No. 0704-0188

1. AGENCY USE ONLY (Leave blank)	2. REPORT DATE	3. REPORT TYPE AND DATES COVERED
	July 15, 1997	Final Technical Report: 6/1/96-5/31/97

4. TITLE AND SUBTITLE
Final Technical Report, ONR No. N00014-96-1-0987
Annual Technical Report, ONR No. N00014-96-1-0987

5. FUNDING NUMBERS
ONR No. N00014-96-1-0987

6. AUTHOR(S)
Thomas E. Barnard and Mark J. Beran

7. PERFORMING ORGANIZATION NAME(S) AND ADDRESS(ES)
Office of Sponsored Programs
The Catholic University of America
Cardinal Station
Washington, DC 20064

8. PERFORMING ORGANIZATION REPORT NUMBER
(None)

9. SPONSORING/MONITORING AGENCY NAME(S) AND ADDRESS(ES)
Office of Naval Research
Program Officer Dr. Jeffrey Simmen ONR 3210A
Ballston Centre Tower One
800 North Quincy Street
Arlington, VA 22217-5660

10. SPONSORING/MONITORING AGENCY REPORT NUMBER
Unknown

11. SUPPLEMENTARY NOTES

12a. DISTRIBUTION/AVAILABILITY STATEMENT
Approved for Public Release
Distribution Unlimited

12b. DISTRIBUTION CODE

13. ABSTRACT (Maximum 200 words)

The objectives of this AASERT grant effort were 1) to incorporate an absorptive bottom into the study of mode energy transfer and decay induced by volume scattering in a shallow channel and 2) to incorporate a piecewise linear sound speed profile into the study of mode energy transfer and decay induced by volume scattering in a shallow channel. Both objectives have been achieved. The introduction of an absorptive bottom generates an additional diffusion term in the coherence range-evolution differential equation and qualitatively changes the nature of the solution. The piecewise linear sound speed profile produces vertical mode wave equation solutions which are Bessel functions with pure imaginary order and pure imaginary argument. These Bessel functions are closely related to the Airy functions Ai and Bi, which are used in their representation. Final results of this effort will be found in Mr. Barnard's doctoral dissertation, which should appear early in 1998.

14. SUBJECT TERMS
Underwater sound scattering, volume scattering, bottom absorption, piecewise linear sound speed profile

15. NUMBER OF PAGES
42

16. PRICE CODE

17. SECURITY CLASSIFICATION OF REPORT	18. SECURITY CLASSIFICATION OF THIS PAGE	19. SECURITY CLASSIFICATION OF ABSTRACT	20. LIMITATION OF ABSTRACT
UNCLASSIFIED	UNCLASSIFIED	UNCLASSIFIED	UL

Subject: Final Technical Report, ONR No. N00014-96-1-0987
June 1, 1996-May 31, 1997

Principal Investigator: Prof. M. J. Beran
The Catholic University of America
E-mail: beran@cua.edu

To: Dr. J. Simmen
Ocean Acoustics
Office of Naval Research
800 N. Quincy St.
Arlington, VA 22217-5000
E-mail: simmenj@onrhq.onr.navy.mil

Date: July 15, 1997

During the contract period, the following topics were considered:

1) Incorporation of an absorptive bottom into the study of mode energy transfer and decay induced by volume scattering in a shallow channel.

2) Incorporation of a piecewise linear sound speed profile into the study of mode energy transfer and decay induced by volume scattering in a shallow channel.

This work is the continuation of work begun under Contract ONR No. N-00014-94-1-0201. All of the research done under the new AASERT grant was conducted by a Ph. D. candidate, Mr. Thomas E. Barnard, under the guidance of the principal investigator, Prof. M. J. Beran. Mr. Barnard wishes to thank Drs. Shimshon Frankenthal and Mark Mirotznik for many helpful suggestions.

1. Incorporation of an absorptive bottom into the study of mode energy transfer and decay induced by volume scattering in a shallow channel.

A summary of the results of this work was presented at the 133rd Meeting of the Acoustical Society of America at State College, Pennsylvania, June 19, 1997, in the paper "The Effect of an Absorptive

Bottom on the Propagation of the Coherence Function in a Shallow-Water Channel," by Tom Barnard and Mark J. Beran. The abstract follows:

When a transverse plane wave propagates through a shallow-water channel with random sound-speed fluctuations, the waveforms at different transverse separations no longer correlate perfectly. The associated coherence falls as the in-line propagation distance and the transverse separation increase. In the (lossless) rigid-bottom case, when the waveforms are represented as a summation of normal modes, the multimodal coherence vector obeys a first-order matrix differential equation with in-line propagation distance as the dependent variable. The scattering matrix in this differential equation is a function of transverse separation. As the in-line propagation distance approaches infinity, the coherence vector approaches a constant vector times a scalar Dirac delta function centered at zero transverse separation. If the bottom is absorptive rather than rigid, an additional diffusion term appears in the matrix partial differential equation governing the coherence. Diffusion along the transverse separation axis then prevents the creation of a Dirac delta function as the in-line propagation distance increases without limit. This diffusion occurs whenever the imaginary part of the horizontal wavenumber component for a particular mode is nonzero. Some graphical outputs depicting the coherence propagation for an absorptive bottom are presented in this paper. [This work was supported by ONR Code 321.]

A copy of this paper will be sent to Dr. Simmen at ONR.

1.1 Development

Given a modal solution

$$\hat{p}(\mathbf{x}) = \sum_{n} \tilde{p}_n(\mathbf{r})\, Y_n(y)$$

to the Helmholtz equation

$$\left[\frac{\partial^2}{\partial y^2} + \frac{\partial^2}{\partial \mathbf{r}^2} + k^2(\mathbf{x})\right] \hat{p}(\mathbf{x}) = 0,$$

where $\hat{p}(x)$ is the complex amplitude of a monochromatic acoustic pressure signal at the frequency ω, $k(\mathbf{x})$ is the corresponding wavenumber at the local sound speed, and the position vector **x** has Cartesian components y (vertical distance from the bottom), z (the in-line propagation direction), x (the transverse direction), and **r** denotes a vector in the horizontal plane (x,z), the vertical mode wave equation becomes

$$\frac{\partial^2 Y_n(y)}{\partial y^2} + \left(k^2 - \beta_n{}^2\right) Y_n(y) = 0$$

if the **average** squared wavenumber in the shallow-water channel is constant and corresponds to a constant sound speed there. Here $k = \omega/c$ is the radian wavenumber, β_n is the horizontal wavenumber for mode n, and $Y_n(y)$ is the pressure for mode n.

Subject to the zero-pressure boundary condition $Y_n = 0$ at the surface and the Newton's law boundary condition

$$\frac{\partial Y_n}{\partial y} = - i k \alpha Y_n$$

at the bottom, where α is the specific acounstic admittance, the resulting eigenvalue equation becomes

$$(\gamma_n h) \cot(\gamma_n h) = i (kh) \alpha,$$

where γ_n is the mode's vertical wavenumber component and h is the channel depth. A graphical solution was given in Morse and Ingard, **Theoretical Acoustics**, Princeton University Press, 1968, pp. 492-506 and p. 909. The solution to this eigenvalue equation was implemented on a digital computer. The principal difficulties were assigning physically reasonable values of γh in the complex plane to specific modes and finding a path from the regularly spaced zeroes of the left-hand side to the value $\gamma_n h$ which solved the eigenvalue equation. (Boundaries between modes passed through saddle points of the function on the left-hand side, and the

saddle point locations for the first twenty modes or so were included in the computer code.)

The coherence function is defined as

$$\left\langle \hat{\Gamma}(x_1,y_1,x_2,y_2,z) \right\rangle = \left\langle \hat{p}(x_1,y_1,z)\, \hat{p}^*(x_2,y_2,z) \right\rangle$$

$$= \sum_m \sum_n \left\langle \Gamma_{mn}(x_1,x_2,z) \right\rangle Y_m(y_1)\, Y_n^*(y_2)\, e^{i\left[\mathrm{Re}(\beta_m - \beta_n)\right] z}$$

where

$$\tilde{p}_n = p_n\, e^{i\,\mathrm{Re}(\beta_n) z}$$

and the self- and cross-modal coherences are defined by

$$\left\langle \Gamma_{mn}(x_1,x_2,z) \right\rangle = \left\langle p_m(x_1,z)\, p_n^*(x_2,z) \right\rangle.$$

In the Beran-Frankenthal scattering model, the self- and cross-modal coherences are a function of (1) the normalized sound speed $c/(\omega h)$, (2) the specific acoustic admittance of the bottom, (3) the strength of the sound speed fluctuations, and (4) the (vertical and horizontal) correlation lengths of the sound speed fluctuations. They also depend on the specific shapes of the correlation functions of the sound speed fluctuations: are they Gaussian or symmetrical exponential cusp shapes, for example?

The coherence measures the expected similarity of the waveform at two different locations and the strength of the waveform. The properties of the coherence function determine when it is no longer practical to increase the size of an acoustic array or beamforming aperture. Scattering can be statistically characterized by the coherence. In the world of signal processing, the coherence is known as the crosspower spectrum between the time series at the two different locations. Taking the wavenumber Fourier transform of the coherence (resolving the wavefield into a superposition of plane waves) generates a frequency-wavenumber spectrum, which represents the strength of angular scattering in the

transverse direction. The wider the coherence peak, the more narrowly confined is the angular scattering. For example, when the process starts with a perfectly coherent plane wave, the coherence is constant as a function of transverse separation when the in-line range is zero, and the wavenumber Fourier transform is a Dirac delta function at zero wavenumber: that means that all the energy is concentrated in a plane wave propagating in the in-line direction. Scattering causes the coherence function to form a peak which initially narrows as the in-line range increases, so that the wavenumber Fourier transform broadens out from the initial Dirac delta function at zero wavenumber: that means that the energy spreads out to a *range* of wavenumber values centered at zero wavenumber or, equivalently, a *range* of propagation directions centered about the in-line direction. As long as the energy is confined to the range $|k| \le \omega/c$, called the *visible region*, the frequency-wavenumber spectrum forms a physically meaningful representation of the scattering.

Random sound speed fluctuations are responsible for the volume scattering studied under this contract. The random fluctuations are given by the representation

$$k^2(\mathbf{x}) = k^2 \left[1 + \mu(\mathbf{x})\right],$$

where k^2 is the mean wavenumber squared and $\mu(\mathbf{x})$ is the random relative variation about this mean. After mathematical manipulations similar to those in M. J. Beran and S. Frankenthal, "Volume Scattering in a Shallow Channel," **J. Acoust. Soc. Am.**, 91(6), June 1992, pp. 3203-3211, we have the coherence range-evolution differential equation

$$\left(\frac{\partial}{\partial z} - \frac{\text{Im}\,\beta_m}{\beta_m\,\beta_m^*} \frac{\partial^2}{\partial s_x^{\,2}} + 2\,\text{Im}\,\beta_m + \delta_{mm} \right) \langle \Gamma_{mm} \rangle + \sum_{k \neq m} \delta_{mk} \langle \Gamma_{kk} \rangle = 0,$$

where z is the in-line propagation distance, s_x is the transverse separation, β_m is the horizontal wavenumber for mode m, δ_{mk} is the scattering matrix element controlling the rate of flow of coherence from mode k to mode m, and $\langle \Gamma_{mm} \rangle$ is the coherence between the mode m waveform at position (x,z) and the mode m waveform at position $(x+s_x,z)$. δ_{mk} is a function of the

transverse separation s_x, while $\langle \Gamma_{mm} \rangle$ is a function of the transverse separation s_x and the in-line propagation distance z. In matrix form,

$$\left(\frac{\partial}{\partial z} - \Lambda_\beta \frac{\partial^2}{\partial s_x^2} + 2\,\mathbf{Im}\,\beta + \mathbf{S} \right) \langle \Gamma \rangle = 0,$$

where Λ_β and **Im** β are diagonal matrices, **S** is a square matrix, and $\langle \Gamma \rangle$ is a column vector of self-modal coherences. The second and third terms inside the parentheses vanish if the bottom is rigid (lossless propagation), and, as a result, the solution for the column vector $\langle \Gamma \rangle$ is a matrix exponential times the initial column vector at z = 0. Energy is preserved at zero transverse separation, while at all other transverse separations, the coherence falls off exponentially with increasing z, the rate of falloff increasing with the magnitude of the transverse separation. Thus, with a rigid bottom, the self-modal coherence vector approaches a scaled Dirac delta function centered at zero transverse separation times a constant column vector. With an absorptive bottom, the second term is a diffusion term. This term prevents the formation of a Dirac delta function at zero transverse separation as the in-line propagation distance increases indefinitely. If there is no scattering, the scattering matrix, which depends on the transverse separation, disappears, the second partial with respect to transverse separation is zero, and each mode decays exponentially with no dependence on transverse separation.

Graphical results are given in Figures 1 through 13. The controlling parameter in the case of an absorptive bottom is the scattering/absorption ratio

$$\delta = \frac{\langle \mu^2 \rangle\, k^2\, \sigma_h}{\mathrm{Im}\,\beta_o} \left(\frac{\ell_v}{h} \right),$$

where $\langle \mu^2 \rangle$ is the refractivity fluctuation variance, $k = \omega/c$ is the radian wavenumber, σ_h is the standard deviation of the Gaussian horizontal refractivity fluctuation correlation function, ℓ_v is the characteristic length of the exponential-cusp vertical refractivity fluctuation correlation

function, h is the channel depth, and β_0 is the (complex-valued) horizontal wavenumber for mode 0. The normalized range in Figures 2 through 13 is

$$\begin{Bmatrix} z \langle \mu^2 \rangle k^2 \sigma_h \left(\ell_v / h \right) \text{ if } \delta \geq 1 \text{ (scattering dominant)} \\ z \operatorname{Im} \beta_0 \text{ if } \delta \leq 1 \text{ (absorption dominant)} \end{Bmatrix},$$

where z is the unnormalized in-line range, while the normalized sound speed is replaced by c/(fh) to create a rational number. In these figures, a "multiscale approximation" is used to generate the coherence values instead of a brute-force numerical solution of the matrix differential equation. This approximation is a truncated matrix series solution to the differential equation: the approximation eventually becomes inaccurate as the in-line propagation distance becomes large, but the in-line range values are kept small enough that the qualitative characteristics of the plots shown are not affected.

The absorptive-bottom results to be presented are for two modes. We have the capability to generate solutions for up to twenty modes, but have not extensively utilized that capability. In the second half of this year, we plan to generate further results with more than two modes.

Figure 1 shows the vertical mode wave equation propagating solutions for a scattering/absorption ratio of 0.04 and a normalized sound speed of one. The imaginary parts of the mode solutions are very small, but not zero. The corresponding solutions for scattering/absorption ratios of one and 25 are not visibly different, so the mode solutions for those values of δ will be omitted later.

With all energy initially concentrated in mode 0, Figure 2 gives mode energy as a function of normalized range for a scattering/absorption ratio of 0.04. No noticeable energy is transferred from mode 0 to mode 1 as in-line range increases. Figure 3 is the same as Figure 2 except that it begins with all energy concentrated in mode 1. The negligible energy transfer from one mode to the other in both these figures reflects the fact that the process is absorption-dominant.

In Figures 4 and 5, the energy is initially equal in both modes. Figure

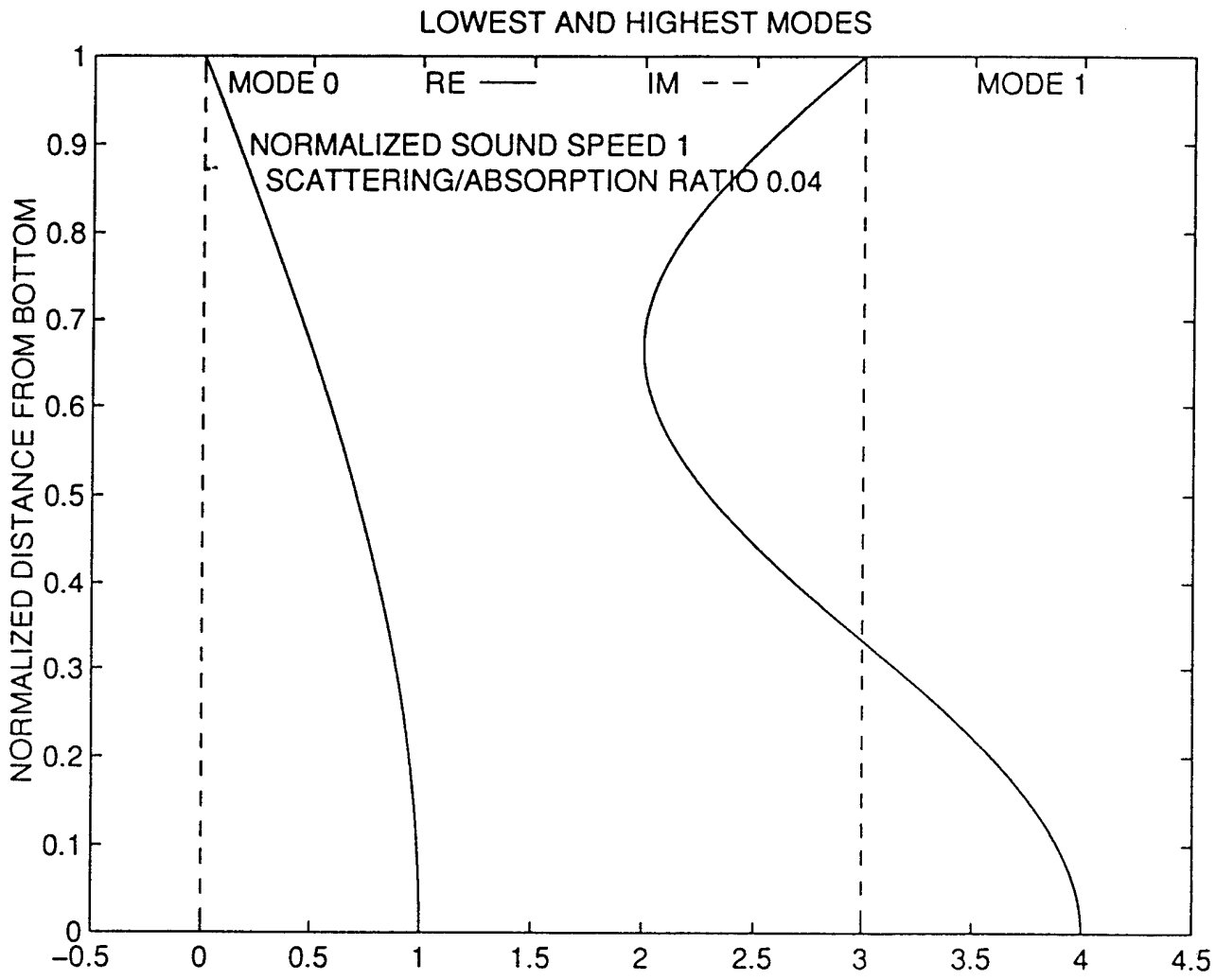

Figure 1. Modes for a Normalized Sound Speed of 1

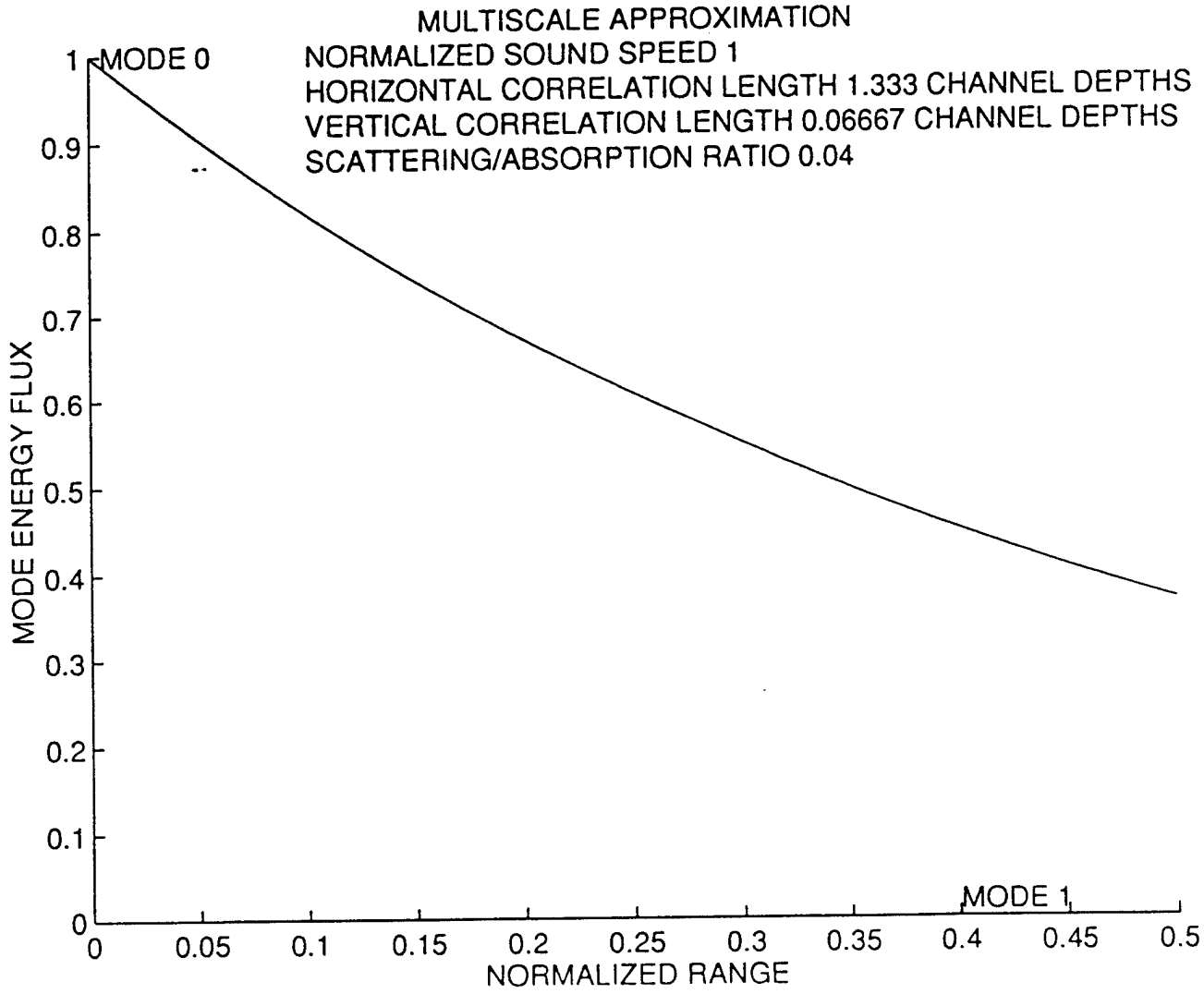

Figure 2. Mode Energy Flux as a Function of Range
for a Scattering/Absorption Ratio of 0.04
with Energy Initially Concentrated in Mode 0

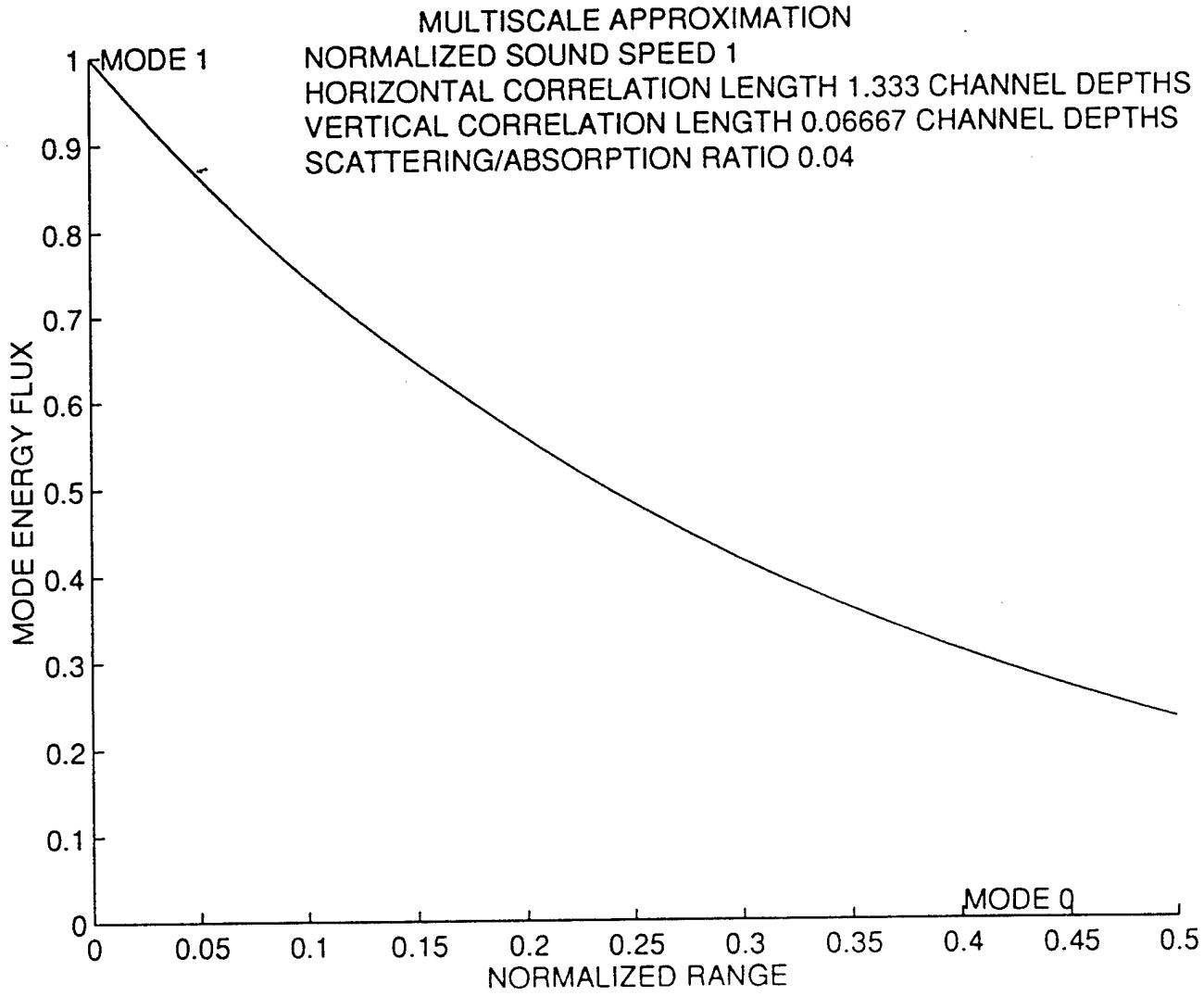

Figure 3. Mode Energy Flux as a Function of Range for a Scattering/Absorption Ratio of 0.04 with Energy Initially Concentrated in Mode 1

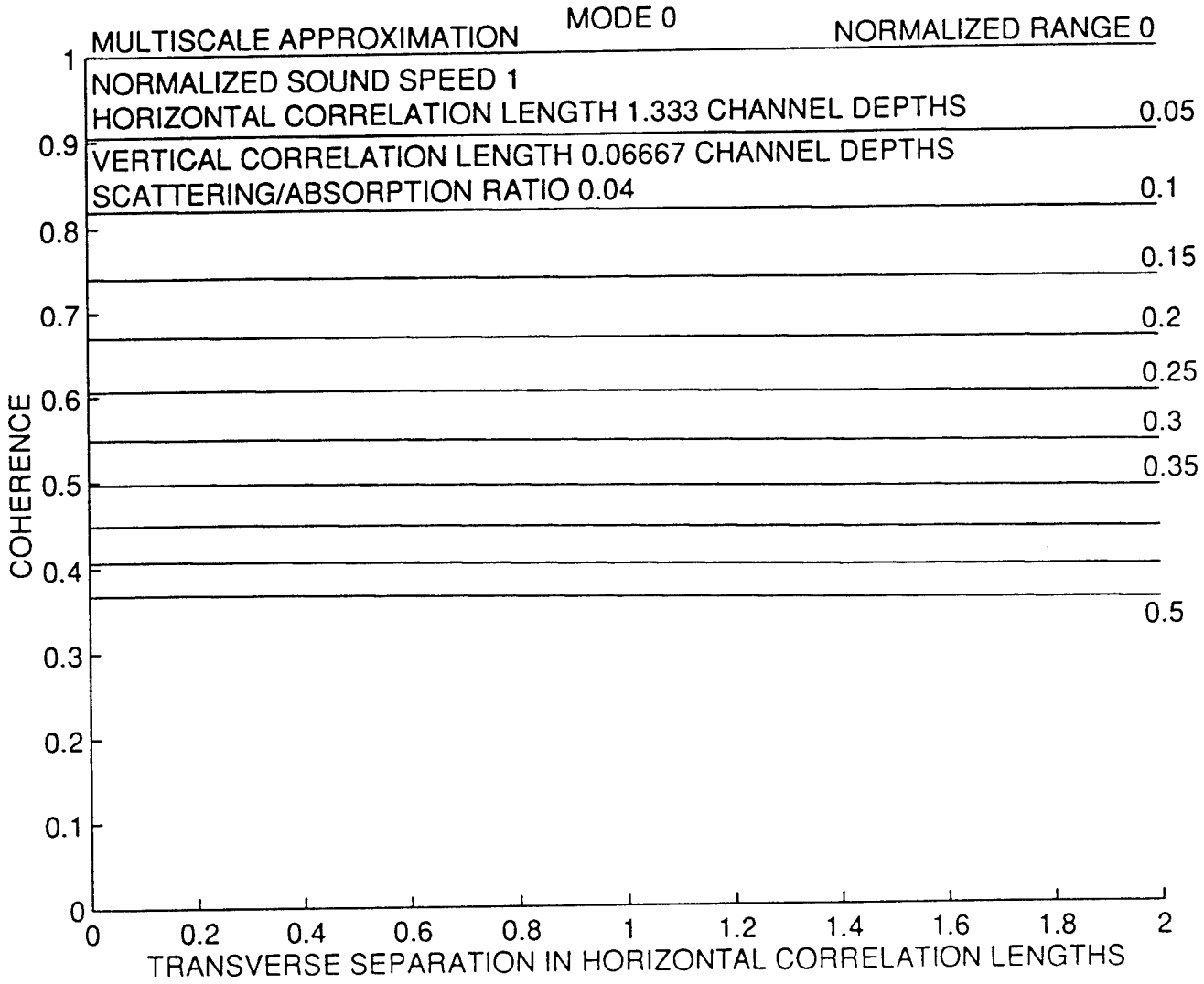

Figure 4. Mode 0 Coherence as a Function of Transverse Separation and Range for a Scattering/Absorption Ratio of 0.04

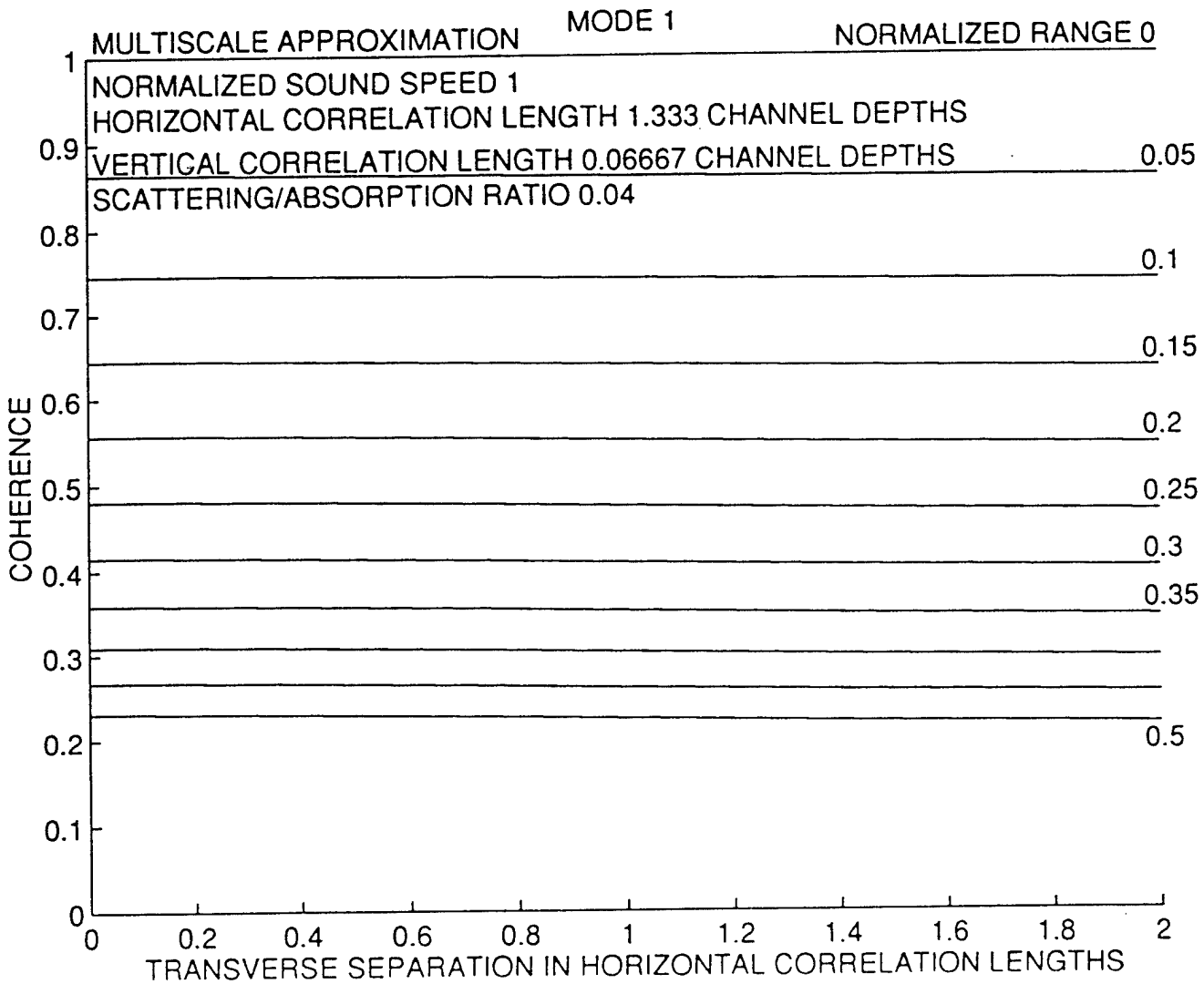

Figure 5. Mode 1 Coherence as a Function of Transverse Separation and Range for a Scattering/Absorption Ratio of 0.04

4 presents mode 0 coherence as a function of transverse separation and range for a scattering/absorption ratio of 0.04. Figure 5 is the same thing for mode 1. In both figures, each curve represents the coherence as a function of transverse separation for one value of range. A careful examination of these figures reveals that there is a barely perceptible peak at zero transverse separation. The fact that it is so hard to see is due to the low scattering/absorption ratio.

Figures 6 through 9 correspond to Figures 2 through 5, but are for a scattering/absorption ratio of one. In Figures 6 and 7, enough energy is transferred from the initial mode to the other mode that it is clearly visible at the maximum range value. In Figures 8 and 9, the effects of scattering are sufficiently strong that the coherence peak at zero transverse separation is clearly visible.

Figures 10 through 13 are for a scattering/absorption ratio of 25. In Figures 10 and 11, the increased energy transfer from the initial mode to the other mode (in comparison with Figures 6 and 7 for $\delta = 1$ and with Figures 2 and 3 for $\delta = 0.04$) is a result of the increased influence of scattering. Figures 12 and 13 depict the coherence as a function of transverse separation and range for modes 0 and 1, respectively. In both figures, the diffusion term in the coherence range-evolution differential equation appears to prevent the creation of a Dirac delta function at zero transverse separation as the normalized range increases indefinitely.

It is useful to compare the absorptive-bottom results just given with the corresponding rigid-bottom results. In the case of a rigid bottom, no energy is dissipated through the water-bottom interface. Likewise, the imaginary part of the vertical mode wave equation eigenfunctions is identically zero. Figures 14 and 15 display the mode energy flux as a function of normalized range when the energy is initially concentrated in mode 0 or in mode 1, respectively. As the normalized range approaches infinity, the mode energy flux approaches a value of one half for both modes. In Figures 16 and 17, as before, the initial energy is equally divided between the two modes. At zero transverse separation, the coherence is one for all range values. At all other transverse separations, it decreases exponentially with range, so that the coherence ultimately approaches a scaled Dirac delta function centered at zero transverse separation as the range goes to infinity. In contrast, for the case of an

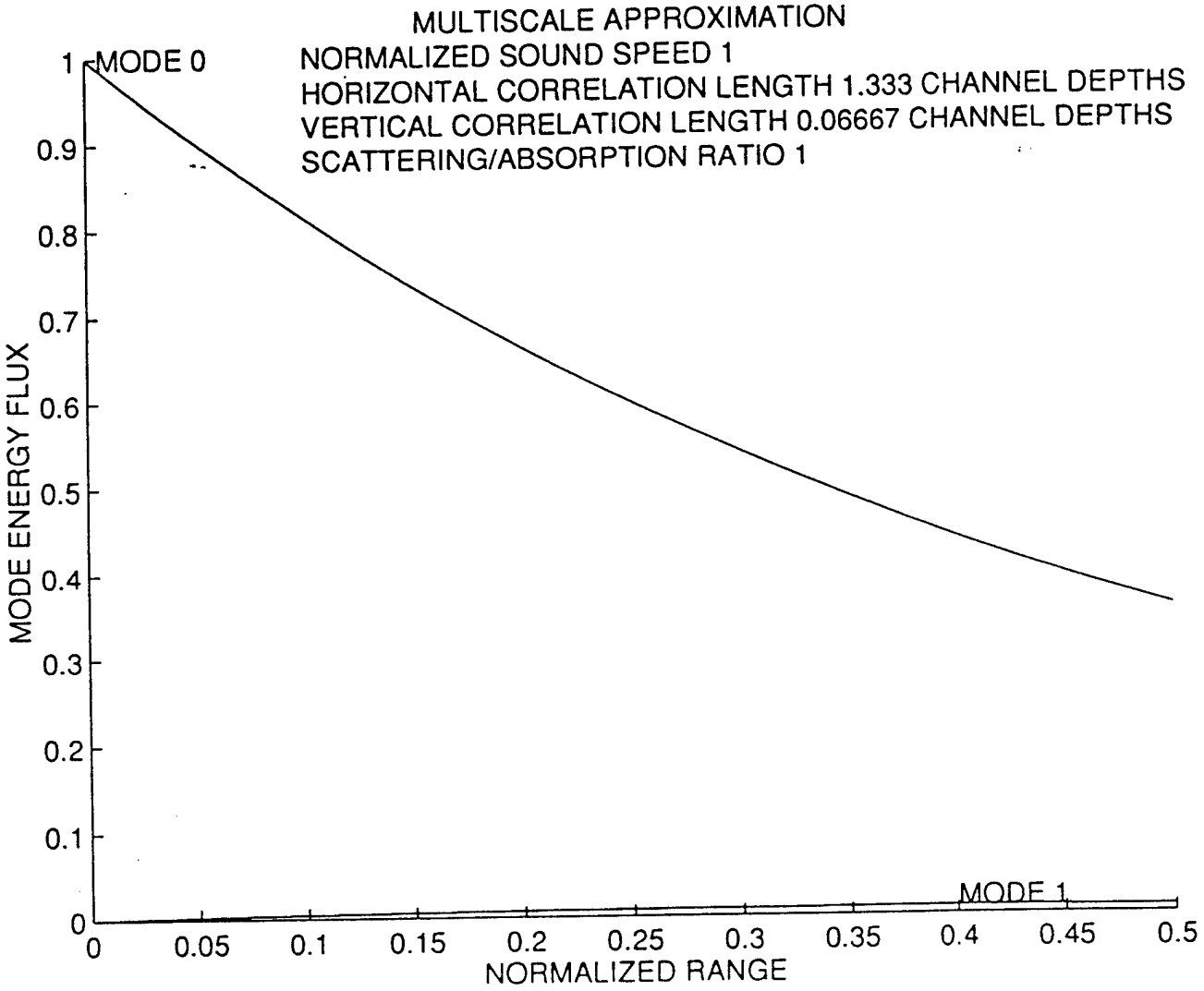

Figure 6. Mode Energy Flux as a Function of Range
for a Scattering/Absorption Ratio of 1
with Energy Initially Concentrated in Mode 0

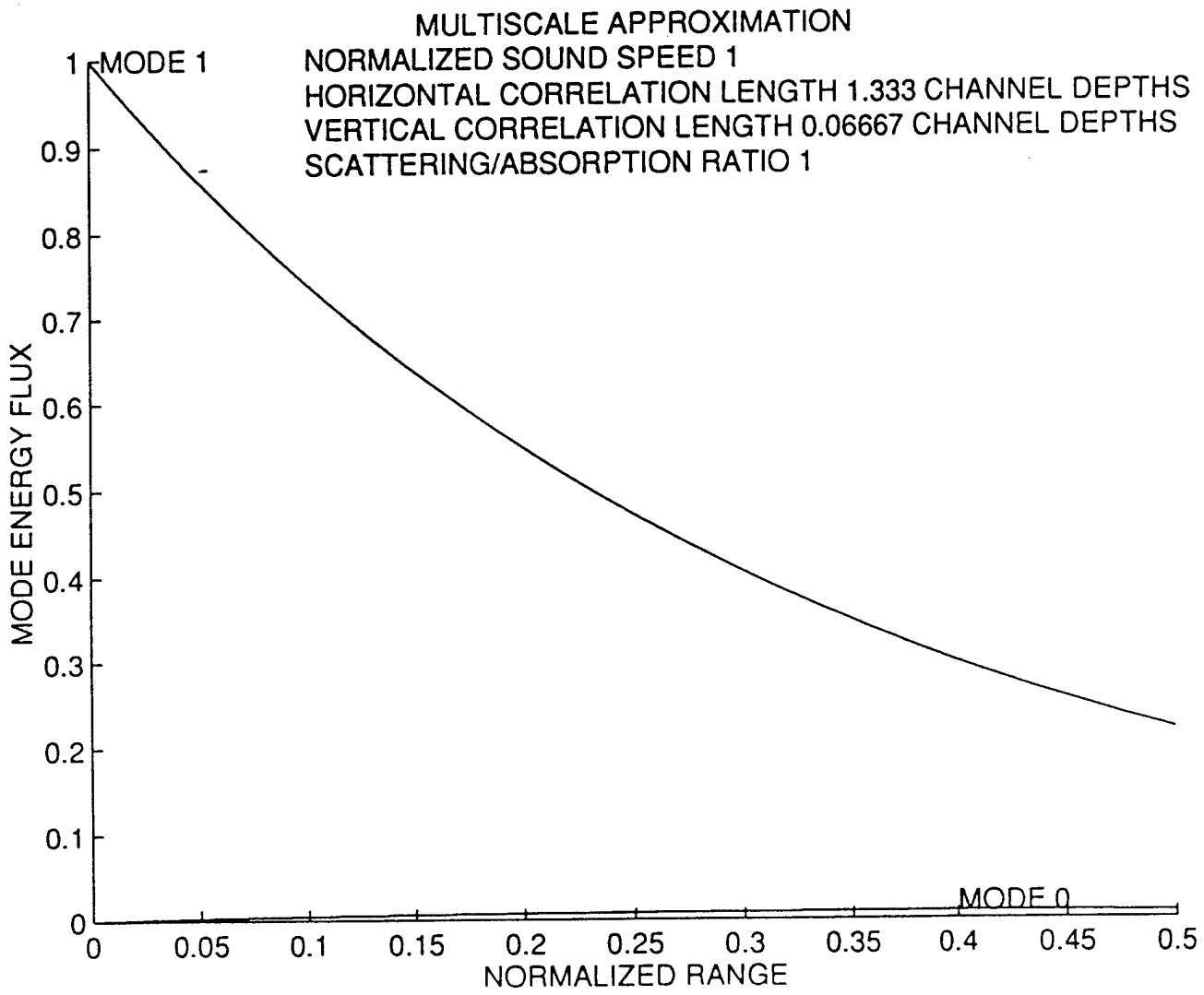

Figure 7. Mode Energy Flux as a Function of Range
for a Scattering/Absorption Ratio of 1
with Energy Initially Concentrated in Mode 0

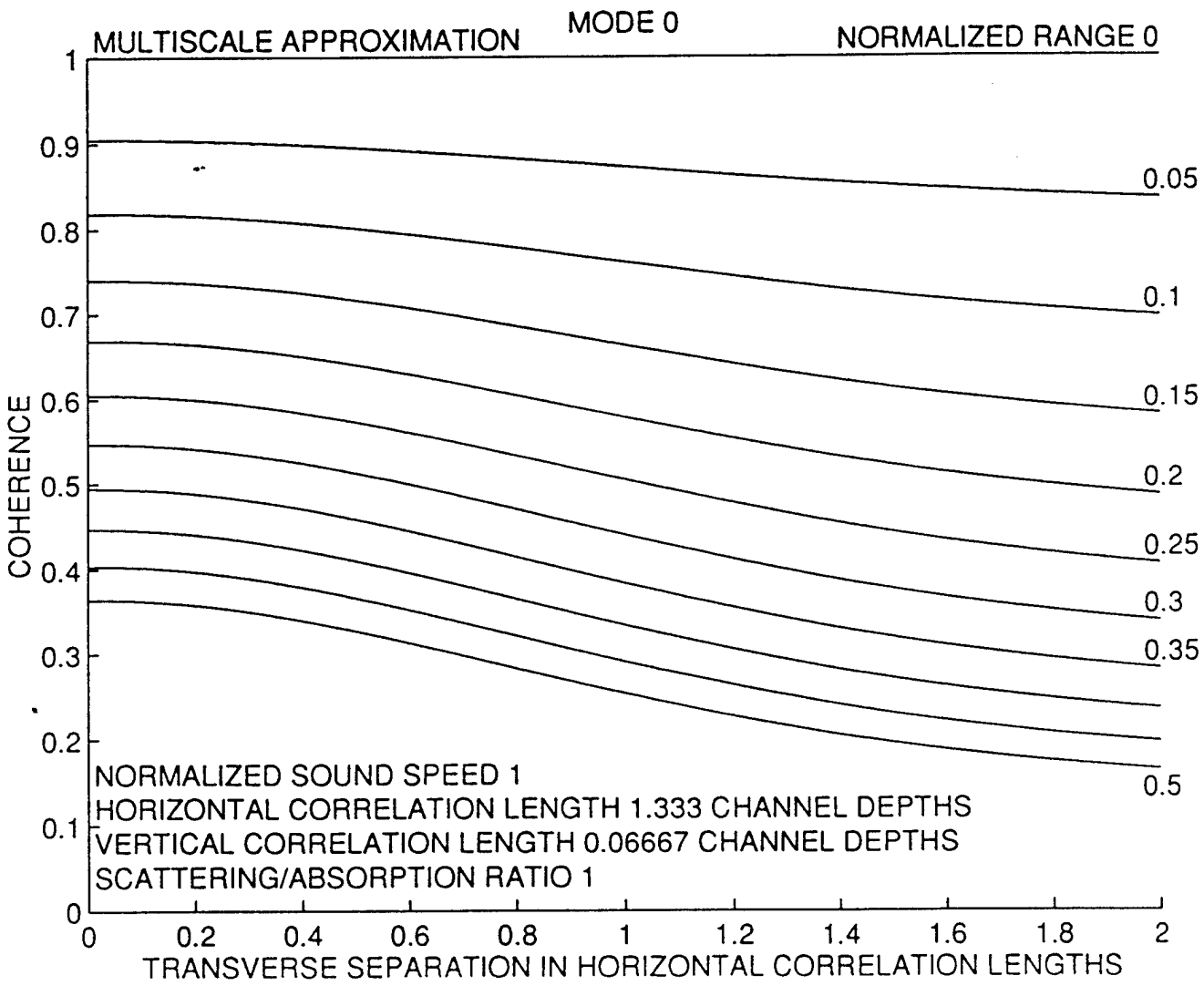

Figure 8. Mode 0 Coherence as a Function of Transverse Separation and Range for a Scattering/Absorption Ratio of 1

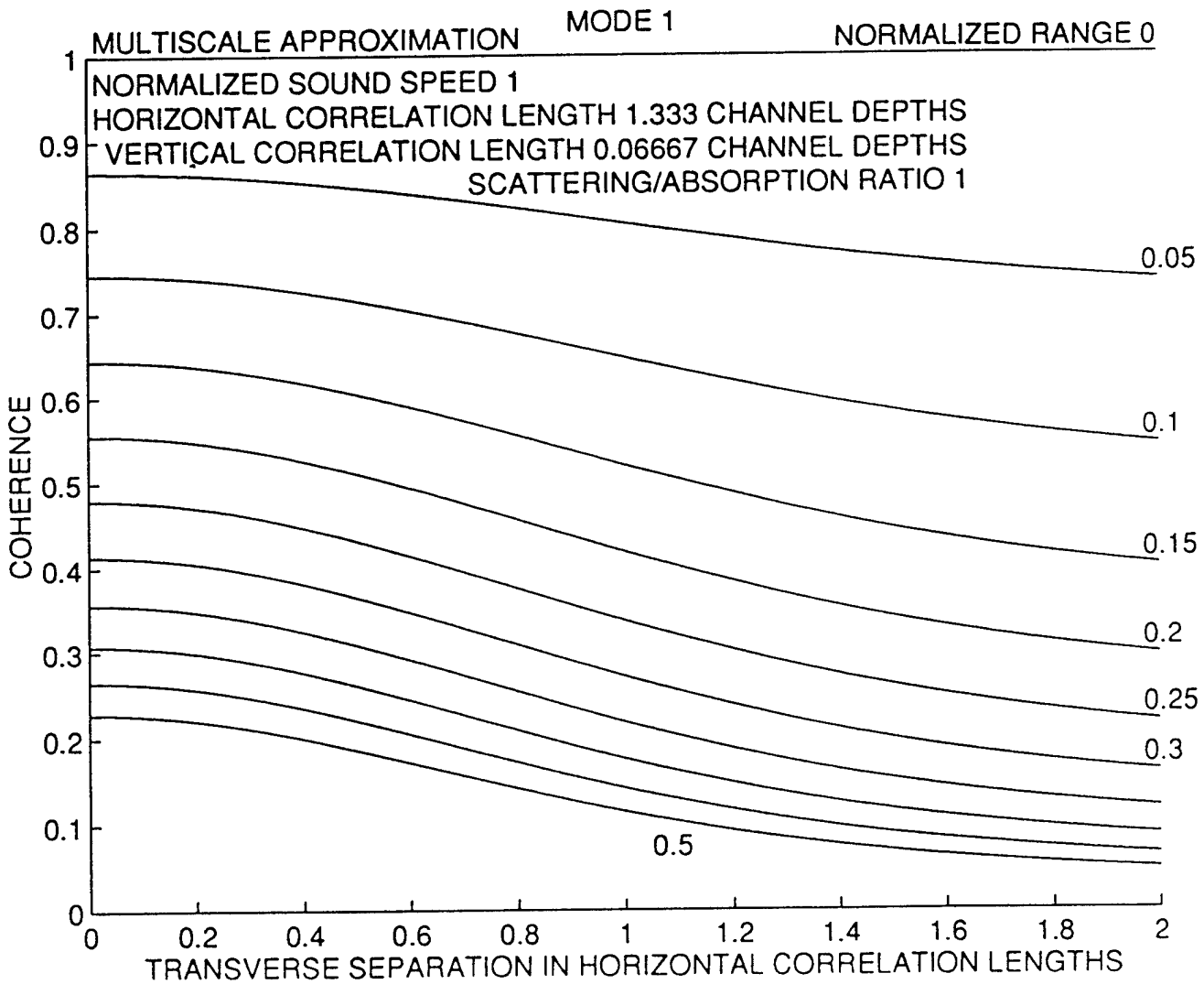

Figure 9. Mode 1 Coherence as a Function of Transverse Separation and Range for a Scattering/Absorption Ratio of 1

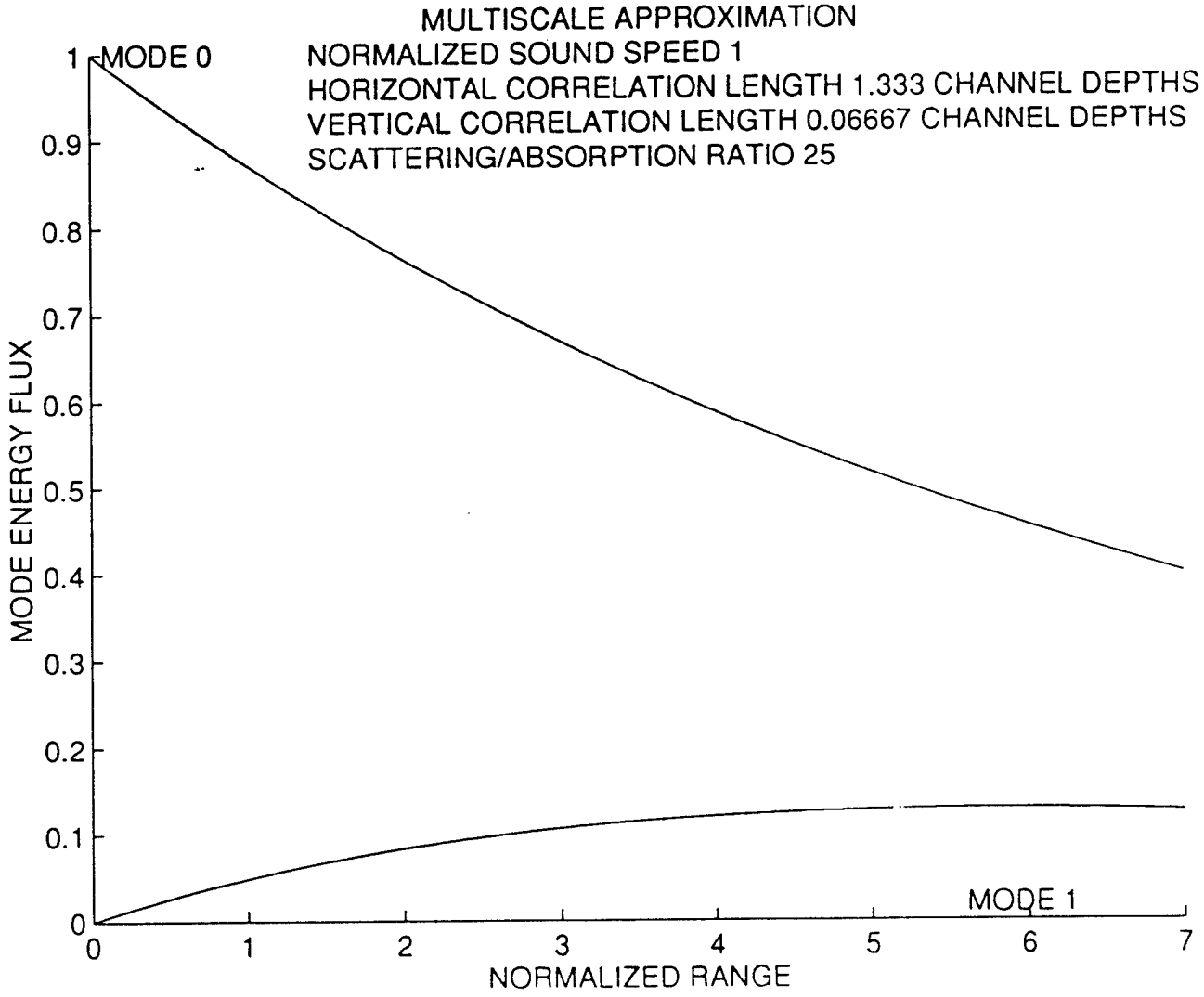

Figure 10. Mode Energy Flux as a Function of Range
for a Scattering/Absorption Ratio of 25
with Energy Initially Concentrated in Mode 0

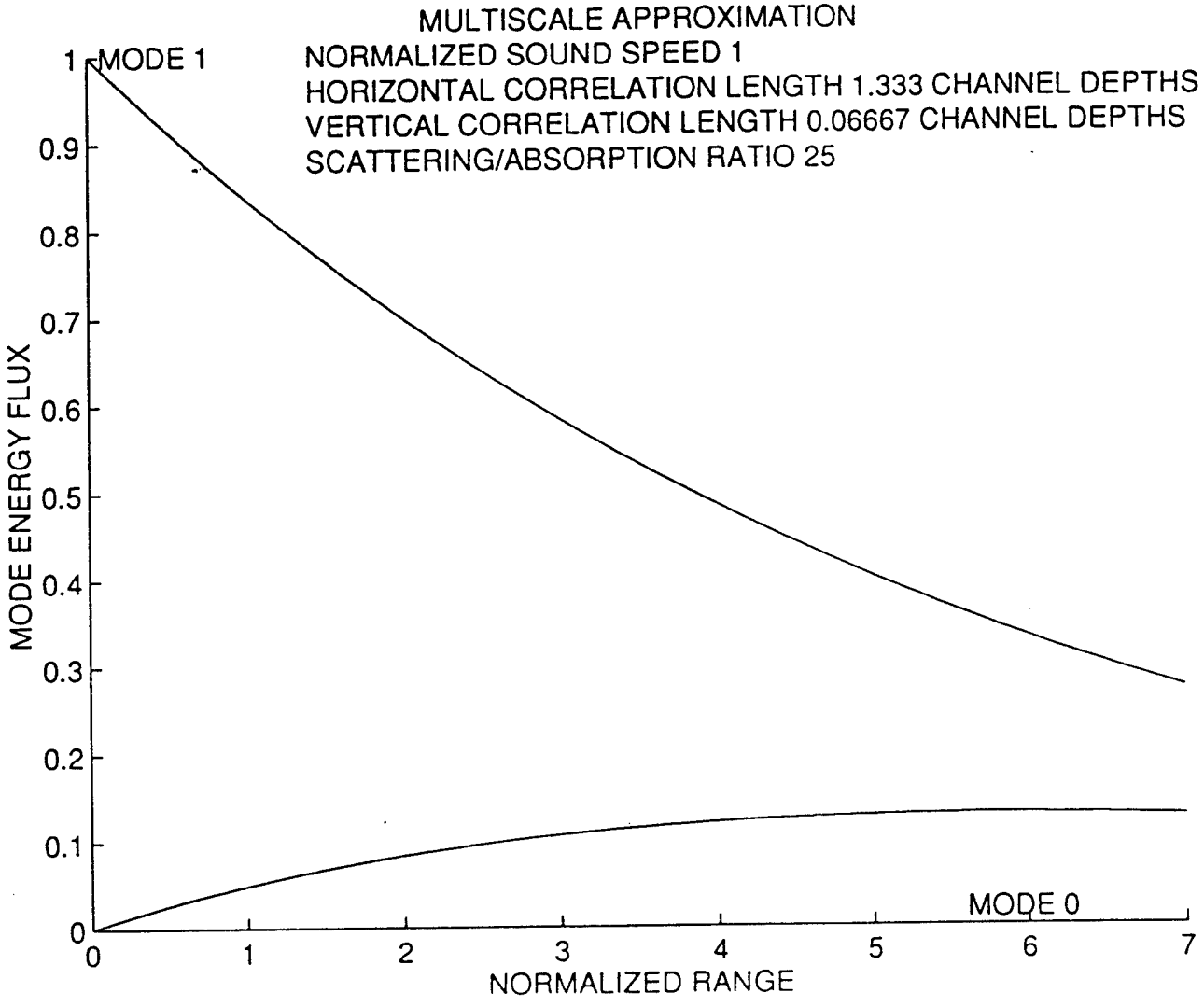

Figure 11. Mode Energy Flux as a Function of Range
for a Scattering/Absorption Ratio of 25
with Energy Initially Concentrated in Mode 1

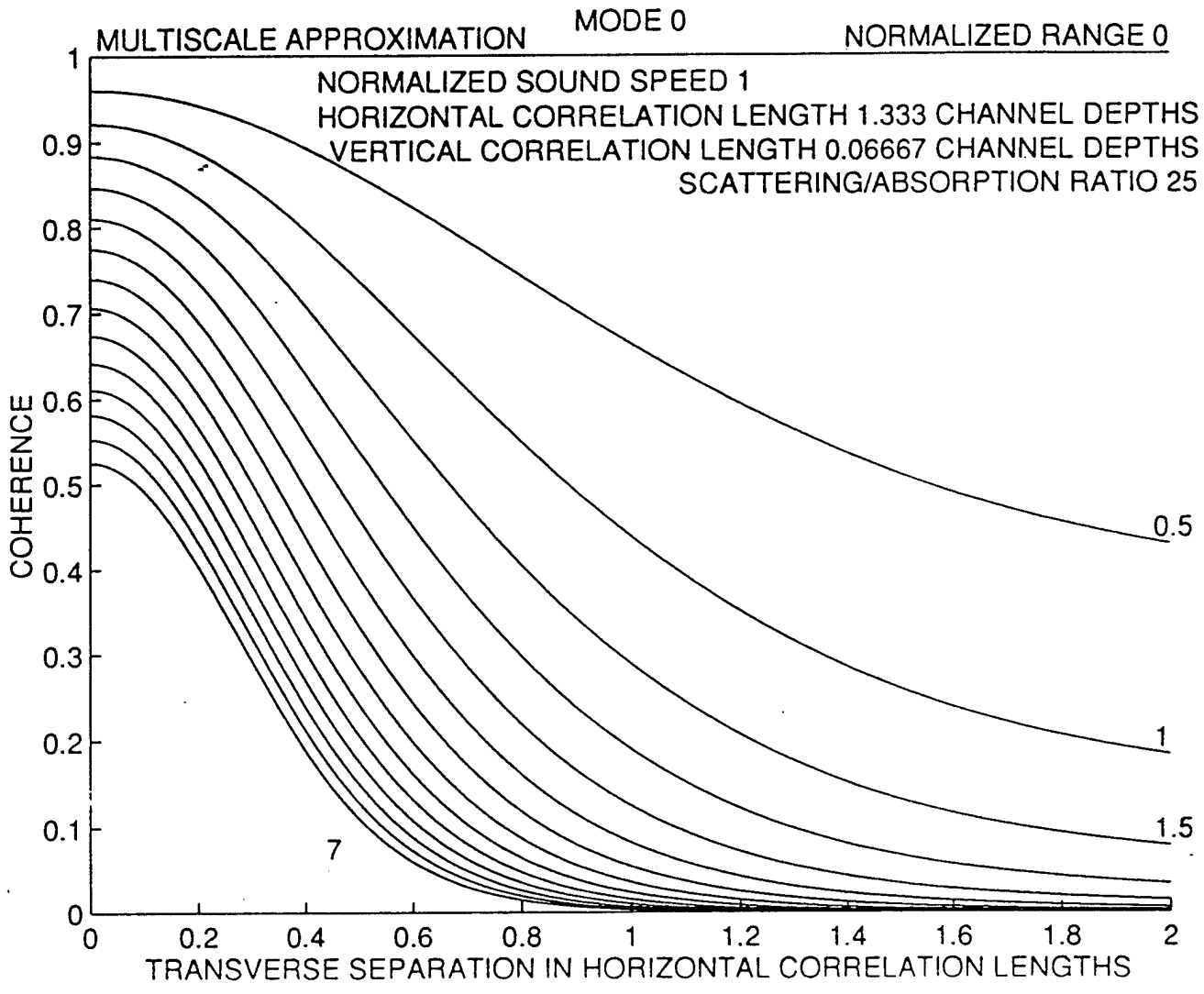

Figure 12. Mode 0 Coherence as a Function of Transverse Separation and Range for a Scattering/Absorption Ratio of 25

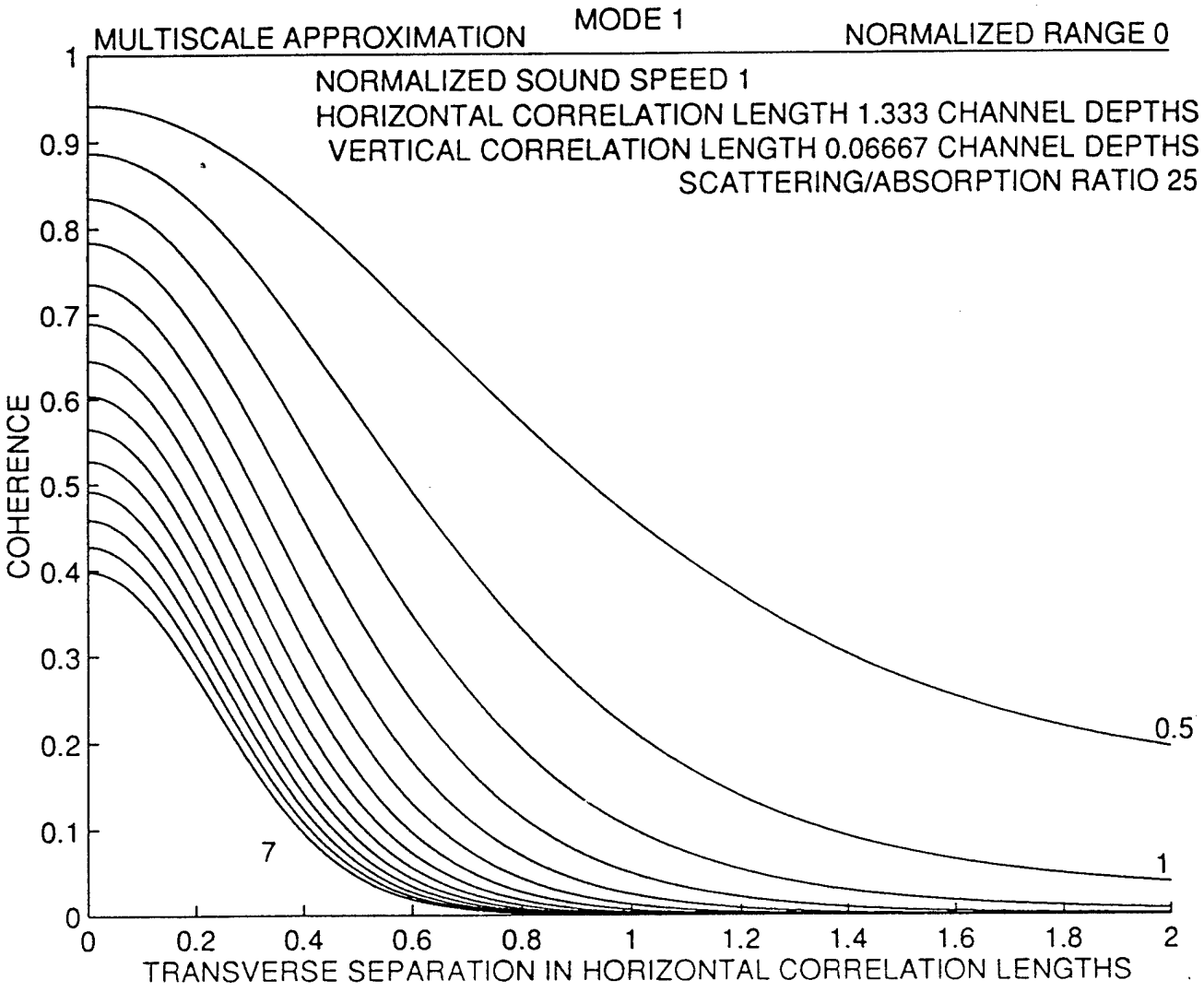

Figure 13. Mode 1 Coherence as a Function of Transverse Separation and Range for a Scattering/Absorption Ratio of 25

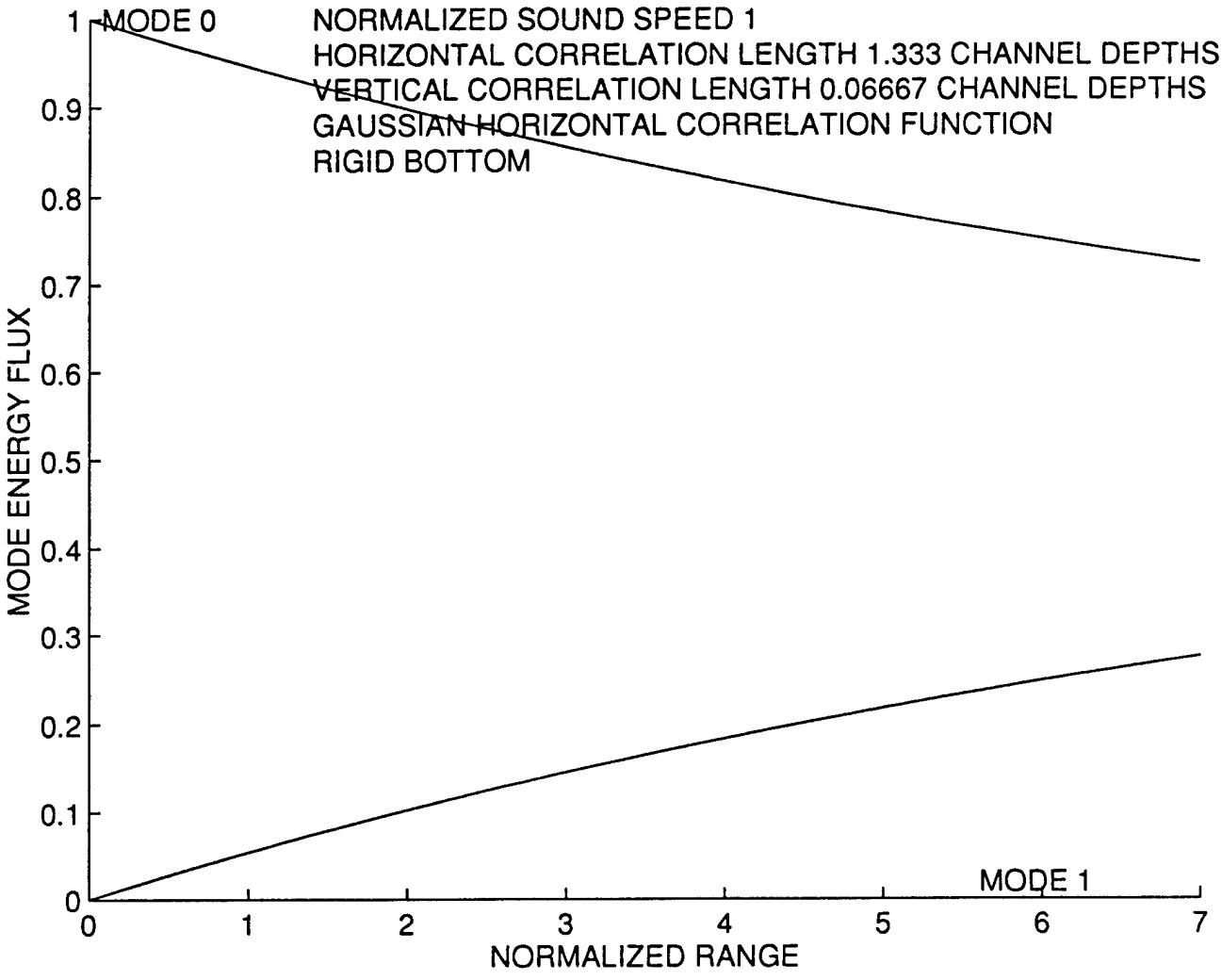

Figure 14. Mode Energy Flux as a Function of Range for a Rigid Bottom with Energy Initially Concentrated in Mode 0

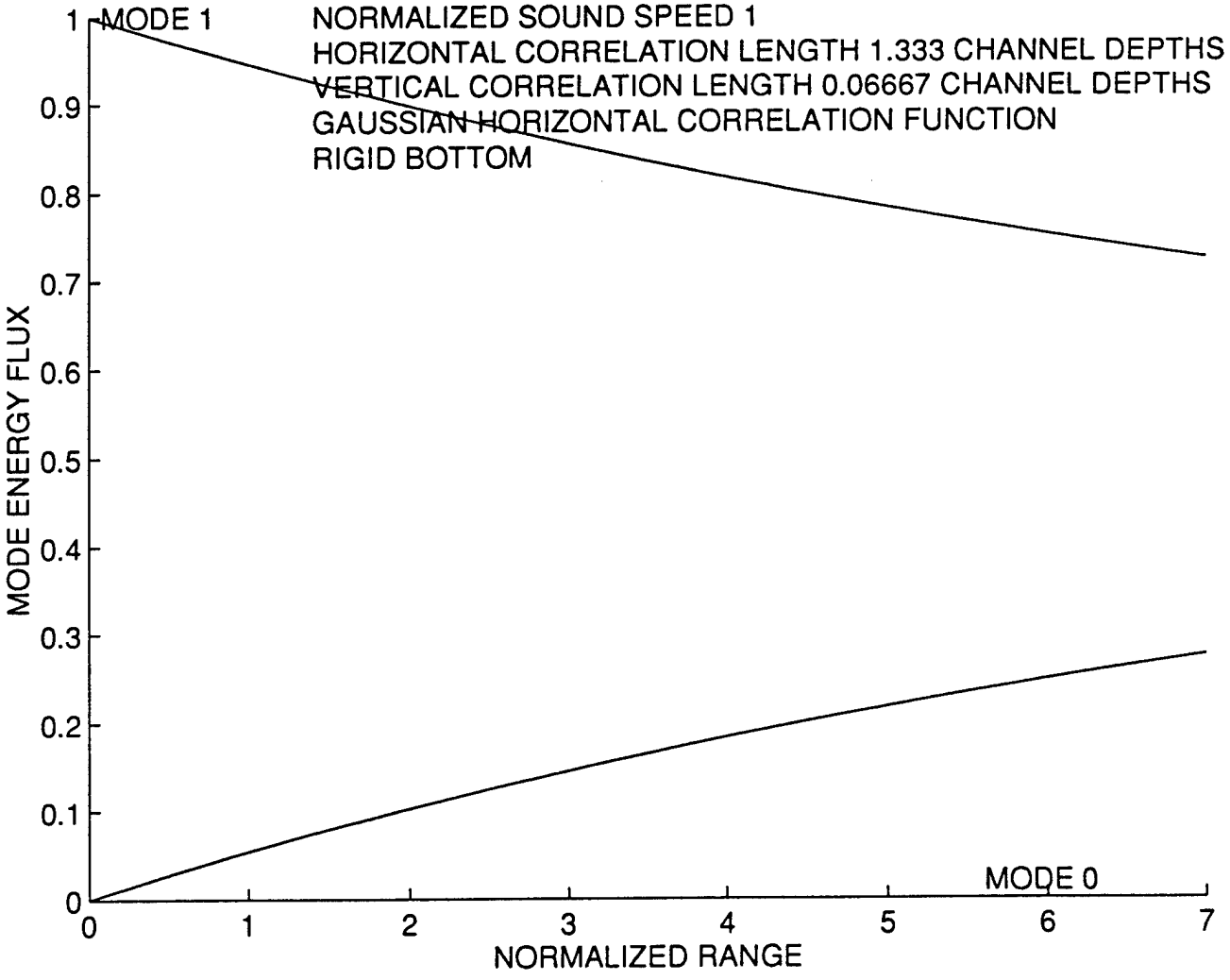

Figure 15. Mode Energy Flux as a Function of Range for a Rigid Bottom with Energy Initially Concentrated in Mode 1

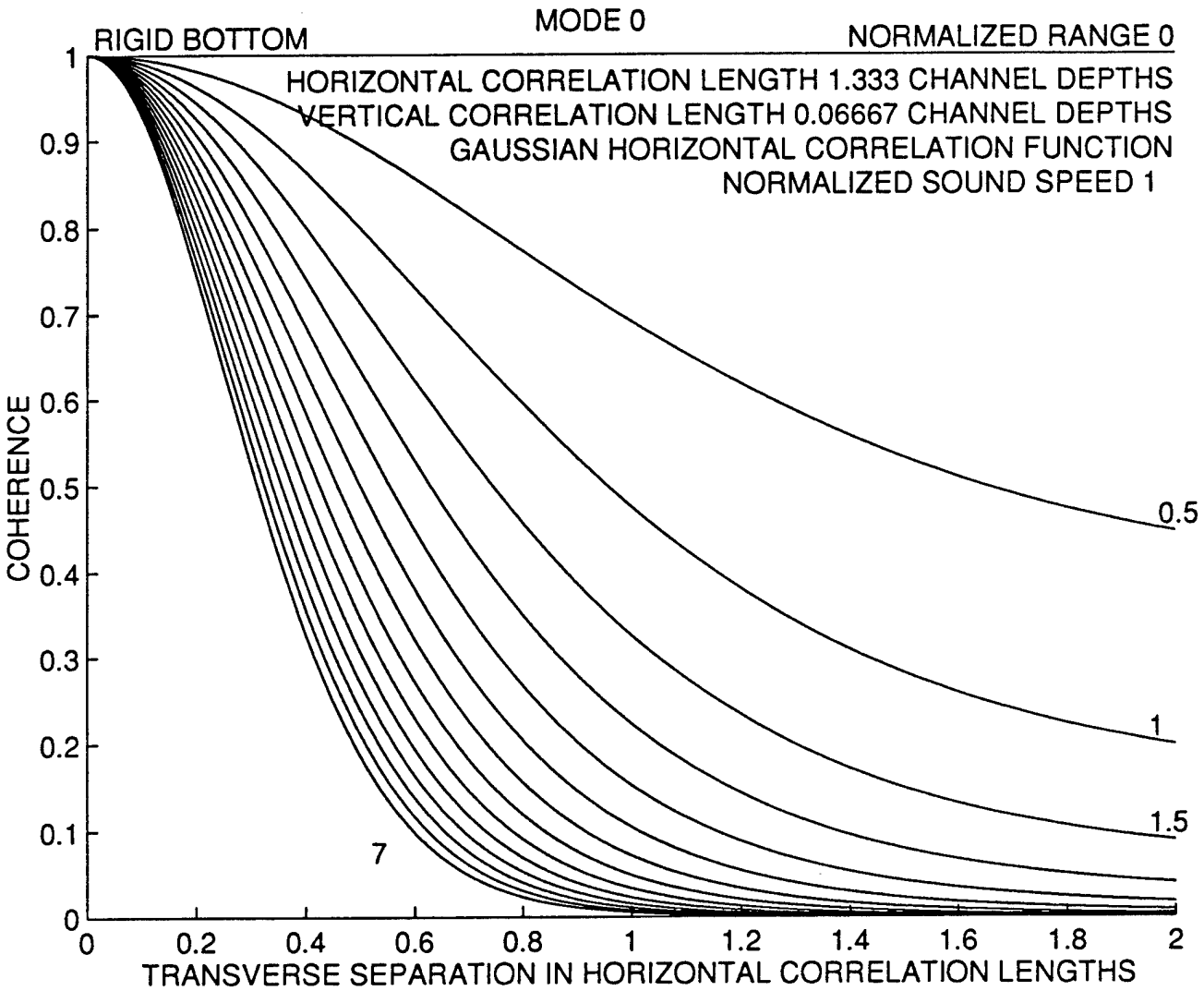

Figure 16. Mode 0 Coherence as a Function of Transverse Separation and Range for a Rigid Bottom

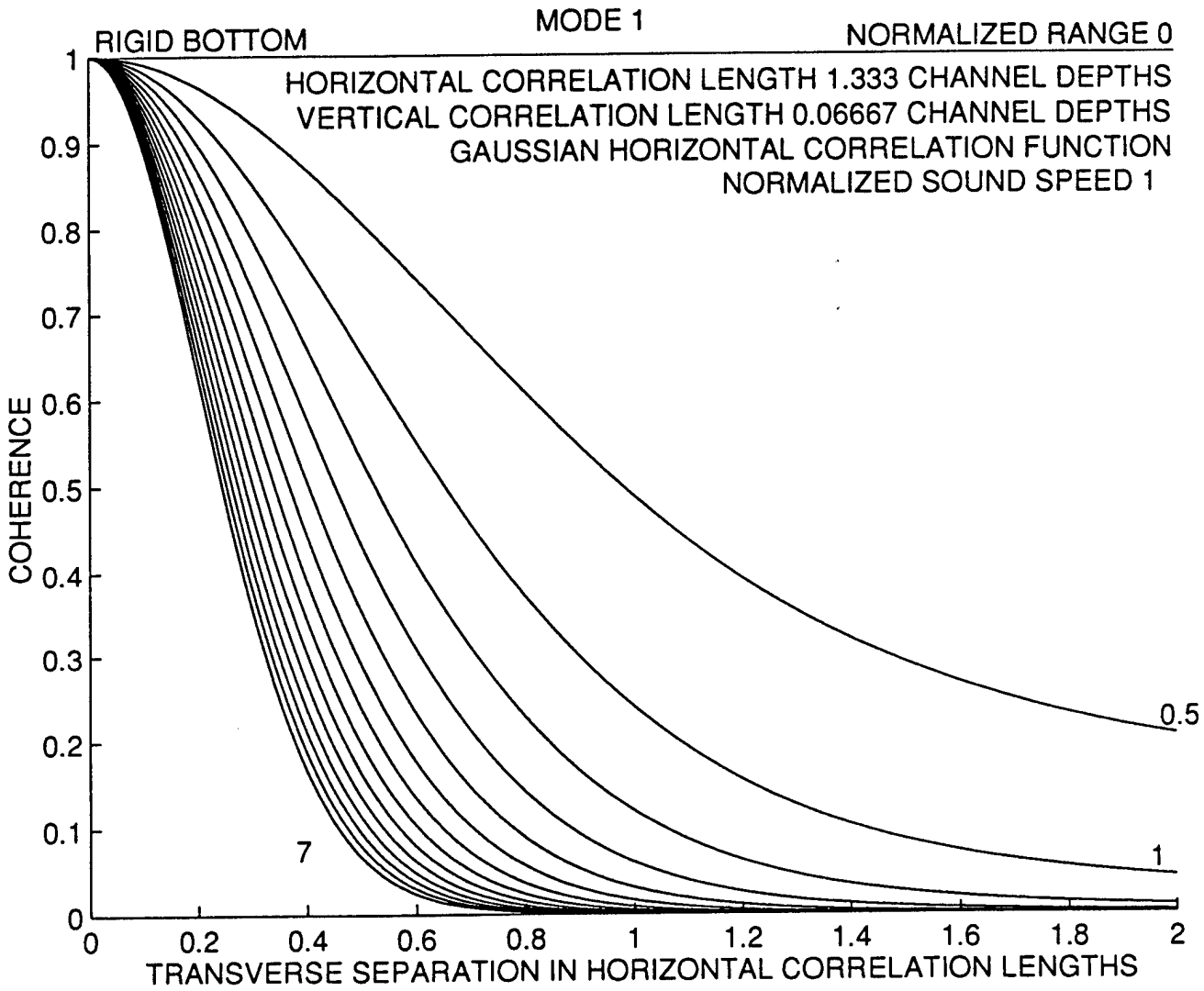

Figure 17. Mode 1 Coherence as a Function of Transverse Separation and Range for a Rigid Bottom

absorptive bottom, the diffusion term in the coherence range-evolution differential equation prevents the formation of infinitely sharp peaks as the range becomes arbitrarily large by diffusing those peaks along the transverse-separation axis.

In the case of a two-dimensional problem, the diffusion term in the coherence range-evolution differential equation disappears, and there is no transverse axis. Figure 18 plots the lowest and highest modes of a twenty-propagating-mode system for a normalized sound speed of 0.1 and a scattering/absorption ratio of 3.508. The mode solutions are sinusoids with one quarter cycle (mode 0) to 9.75 cycles (mode 19), increasing by one half cycle as the mode index increments by one. The imaginary parts of these mode solutions are close to zero. For a two-dimensional system with energy initially concentrated in mode 0, Figure 19 graphs the mode energy flux as a function of range for a scattering/absorption ratio of 3.508.

2. Incorporation of a piecewise linear sound speed profile into the study of mode energy transfer and decay induced by volume scattering in a shallow channel.

When the sound speed is a linear function of depth, the vertical mode wave equation becomes

$$\frac{\partial^2 Y_n(y)}{\partial y^2} + \left[\frac{\omega^2}{(c_o + gy)^2} - \beta_n{}^2\right] Y_n(y) = 0,$$

where c_o is the sound speed at the bottom (y = 0), g is the sound speed gradient, and y is the vertical distance from the bottom. The distance from the bottom to the surface is h. The general solution to this equation is given by

$$Y_n(y) \Big/ \left(1 + \frac{g}{c_o} y\right)^{1/2} =$$

$$C_1 \, \mathrm{Re}\left\{i \, J_{iv}\left[i \, \beta_n\left(\frac{c_o}{g} + y\right)\right]\right\} + C_2 \, \mathrm{Im}\left\{i \, J_{iv}\left[i \, \beta_n\left(\frac{c_o}{g} + y\right)\right]\right\},$$

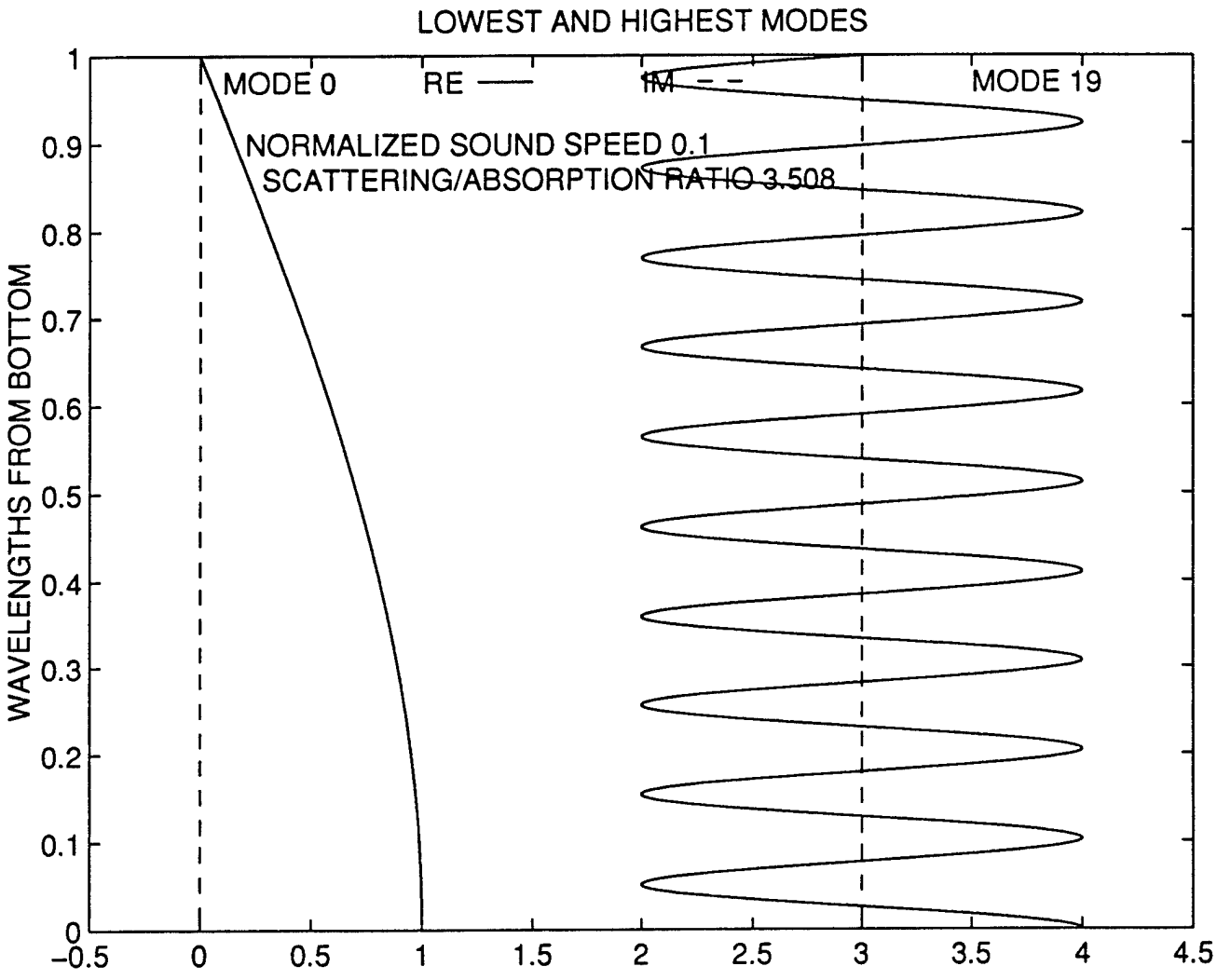

Figure 18. Lowest and Highest Modes for a Normalized Sound Speed of 0.1 and a Scattering/Absorption Ratio of 3.508

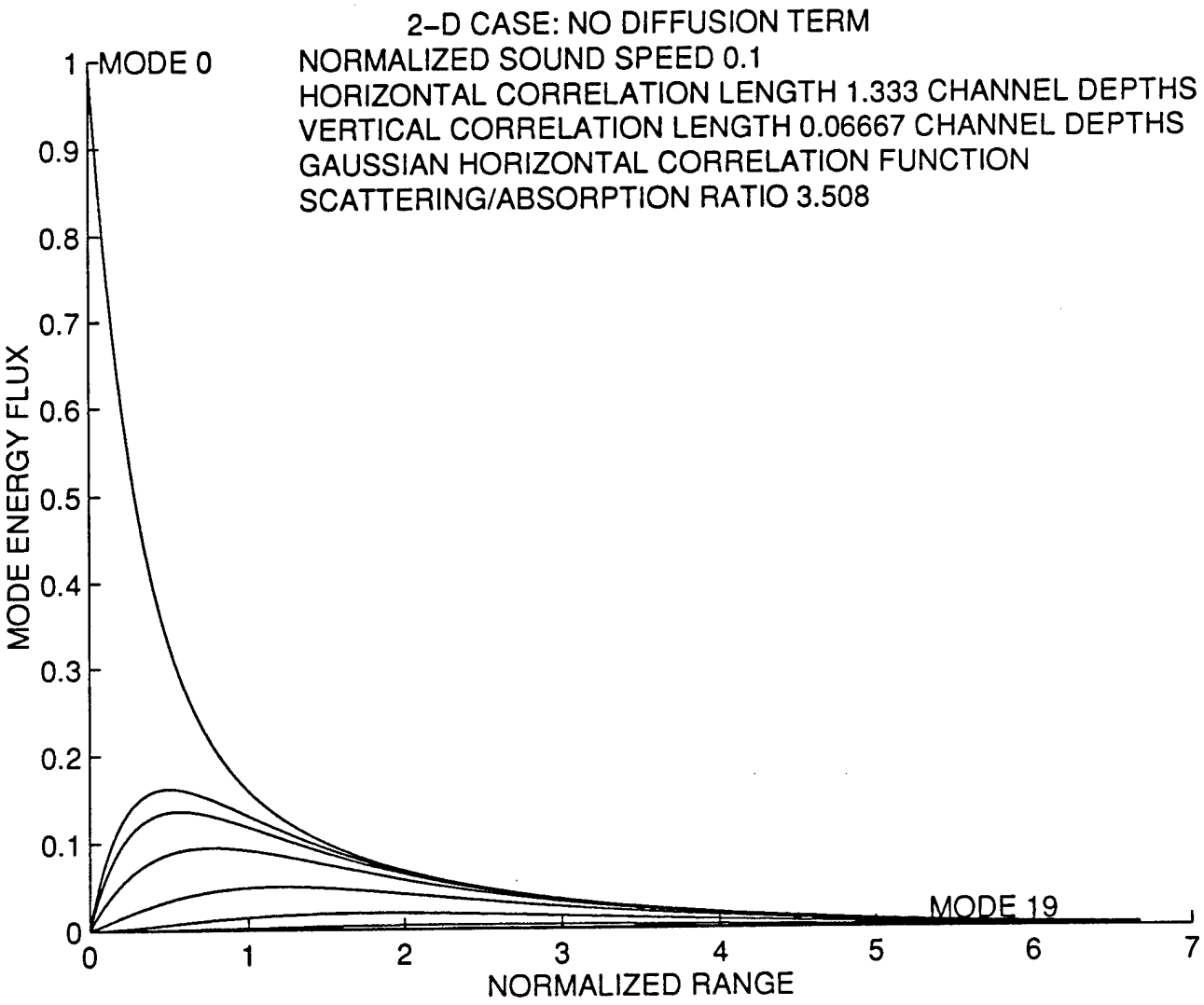

Figure 19. Mode Energy Flux as a Function of Range for a Scattering/Absorption Ratio of 3.508 with Energy Initially Concentrated in Mode 0 in the Two-Dimensional Case with No Diffusion Term

where $iv = i\,[(\omega/g)^2 - 1/4]^{1/2}$ is the pure imaginary order of the complex-valued Bessel function J_{iv}. The real and imaginary parts of $i\,J_{iv}$ are closely related to the Airy functions Ai and Bi, respectively. The choice of Re ($i\,J_{iv}$) and Im ($i\,J_{iv}$) for the two independent solutions instead of I_{iv} and K_{iv} produces independent solutions with comparable envelope magnitudes. The general solution to the differential equation has been given previously in the literature by A. O. Williams, Jr. and Douglas R. MacAyeal, "Acoustic reflection from a sea bottom with linearly increasing sound speed," **J. Acoust. Soc. Am.**, vol. 66, no. 6, Dec 1979, pp. 1836-1841, Leonid M. Brekhovskikh, **Waves in Layered Media**, Academic Press, New York, 1960, p.449, and S. M. Rytov and F. S. Yudkevich, "Electromagnetic wave reflection from a layer with a negative dielectric constant," **Journal of Experimental and Theoretical Physics** [U.S.S.R.], vol. 10, p. 285, [1946].

The boundary conditions for this problem are the zero-pressure condition at the surface (y = h) and the general bottom impedance condition

$$\frac{dY_n/dy}{Y_n} = -i\,k(y)\,\Big|_{y=0}\,\alpha = -i\,\frac{\omega}{c_o}\,\alpha$$

at y = 0, where $\alpha = \xi - i\sigma$ is the specific acoustic admittance, ξ is the specific conductance, and σ is the specific susceptance. These boundary conditions lead to the eigenvalue equation

$$0 = \left\{ h\,\frac{d}{dy}\,\mathrm{Re}\left[i\,J_{iv}\left(i\,\frac{\beta_n\,c_o}{g} \right) \right] + \left[i\,\frac{(\omega/c_o)}{\beta_n}\,\alpha + \frac{1}{2}\left(\frac{g}{\beta_n\,c_o} \right) \right] \mathrm{Re}\left[i\,J_{iv}\left(i\,\frac{\beta_n\,c_o}{g} \right) \right] \right\} \mathrm{Im}\left[i\,J_{iv}\left(i\,\frac{\beta_n\,c_s}{g} \right) \right]$$

$$- \left\{ h\,\frac{d}{dy}\,\mathrm{Im}\left[i\,J_{iv}\left(i\,\frac{\beta_n\,c_o}{g} \right) \right] + \left[i\,\frac{(\omega/c_o)}{\beta_n}\,\alpha + \frac{1}{2}\left(\frac{g}{\beta_n\,c_o} \right) \right] \mathrm{Im}\left[i\,J_{iv}\left(i\,\frac{\beta_n\,c_o}{g} \right) \right] \right\} \mathrm{Re}\left[i\,J_{iv}\left(i\,\frac{\beta_n\,c_s}{g} \right) \right],$$

where c_s is the surface sound speed. Solutions exist only for a discrete set of complex values of the normalized horizontal wavenumber values $\beta_n h$. The corresponding mode solutions are given by

$$Y_n(y) / \left(1 + \frac{g}{c_o} y\right)^{1/2} =$$

$$\mathrm{Im}\left\{ i\, J_{iv}\left[i\, \beta_n \left(\frac{c_o}{g} + h \right) \right] \right\} \mathrm{Re}\left\{ i\, J_{iv}\left[i\, \beta_n \left(\frac{c_o}{g} + y \right) \right] \right.$$

$$\left. - \mathrm{Re}\left\{ i\, J_{iv}\left[i\, \beta_n \left(\frac{c_o}{g} + h \right) \right] \right\} \mathrm{Im}\left\{ i\, J_{iv}\left[i\, \beta_n \left(\frac{c_o}{g} + y \right) \right] \right\}.$$

For the case of a linear sound speed profile, the only other important difference from the case of a constant sound speed medium occurs in determining the quadruply-subscripted quantities

$$\sigma_{ijkm}(\mathbf{r}',\mathbf{r}'') = \langle \mu_{ij}(\mathbf{r}')\, \mu_{km}(\mathbf{r}'') \rangle =$$

$$\int_0^h \int_0^h k^2(y')\, Y_i(y')\, Y_j(y')\, \sigma(\mathbf{x}',\mathbf{x}'')\, Y_k(y'')\, Y_m(y'')\, k^2(y'')\, dy''\, dy'$$

needed in evaluating the scattering matrix elements. Here $\sigma(\mathbf{x}',\mathbf{x}'')$ is the refractivity-fluctuation covariance between the two positions $\mathbf{x}'$ and $\mathbf{x}''$. Since the squared wavenumber k^2 is no longer constant, the double integral must be evaluated numerically. Because of symmetries in the integrand, the numerical computations are only slightly more difficult than for a single integral. At the same time, since a numerical integration must be performed, considerably more flexibility is possible in the choice of the refractivity-fluctuation covariance function.

Figure 20 portrays the twenty propagating vertical mode functions for a rigid-bottom case ($\alpha = 0$) when the normalized bottom speed is $c_o/(fh) = 0.0975$ and the normalized surface speed is $c_s/(fh) = 0.1025$. Note that a few of the lower mode functions decay exponentially as the distance from the bottom increases. For the same case, with all energy initially concentrated in mode 0, Figure 21 presents mode energy flux as a function of normalized range. Eventually, as range increases indefinitely, all modes approach identically equal energy flux. In Figures 22 and 23, all twenty

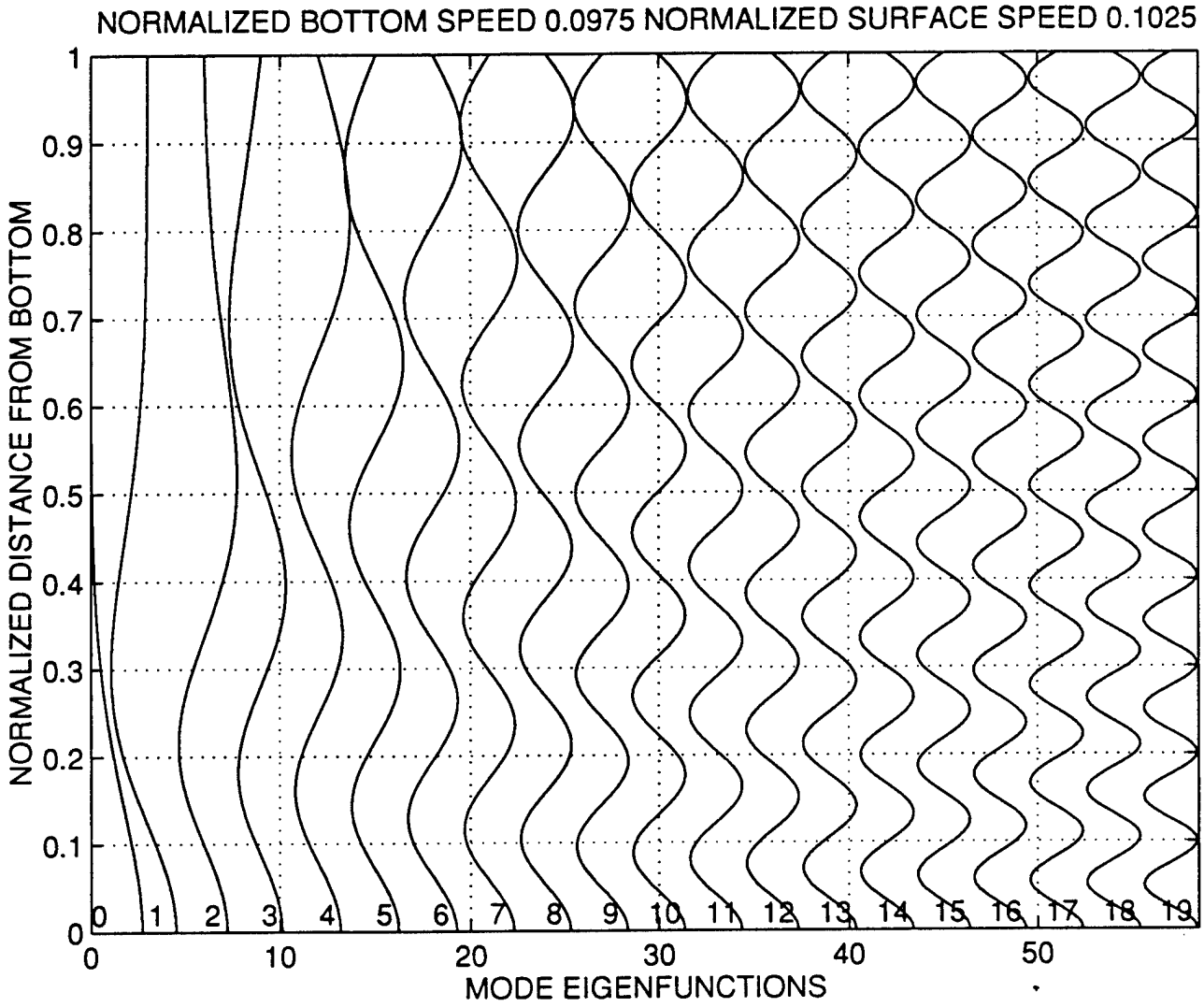

Figure 20. Rigid-Bottom Vertical Mode Functions
for a Normalized Bottom Speed of 0.0975
and a Normalized Surface Speed of 0.1025

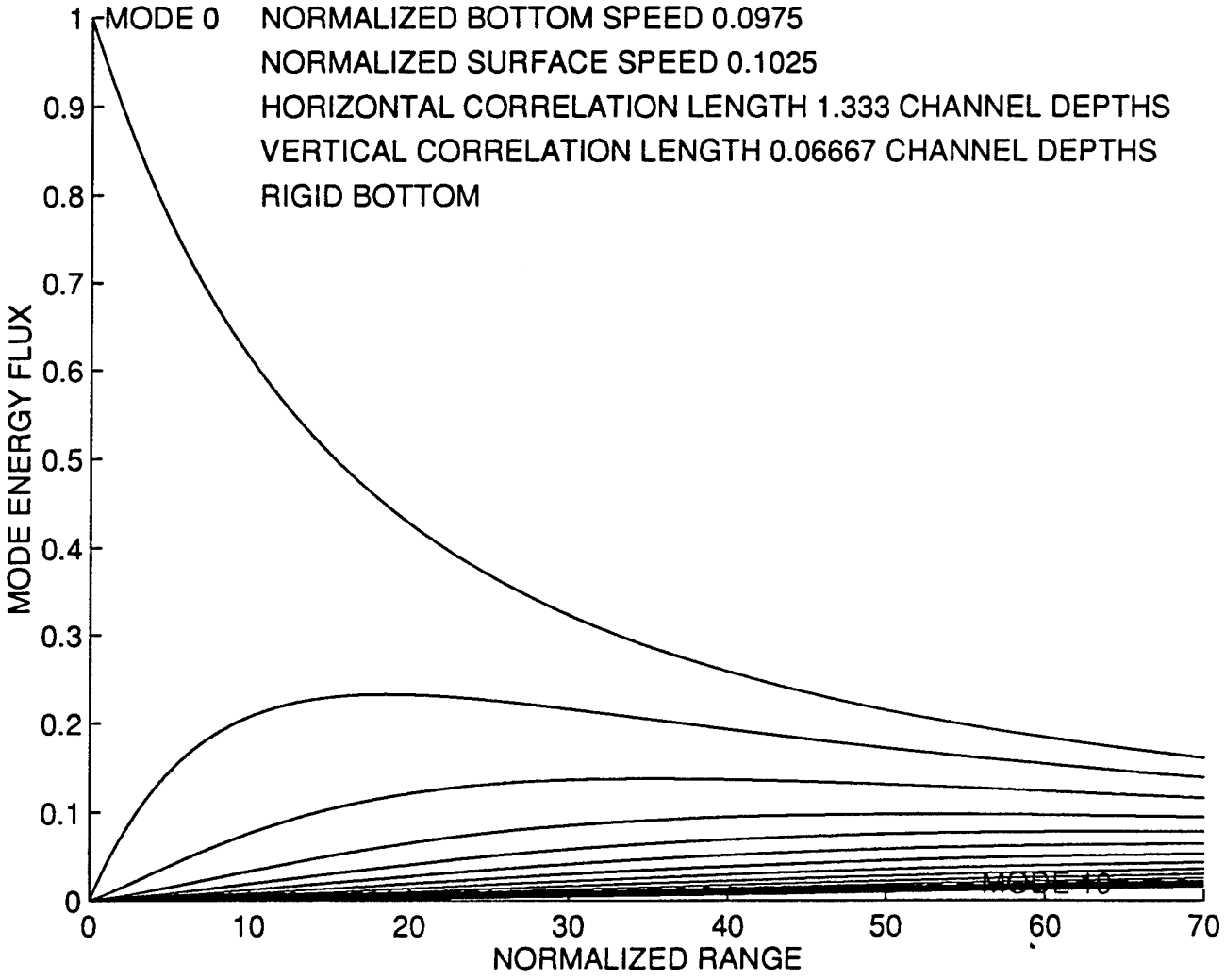

Figure 21. Mode Energy Flux as a Function of Range for a Rigid Bottom, a Normalized Bottom Speed of 0.0975, and a Normalized Surface Speed of 0.1023 with Energy Initially Concentrated in Mode 0

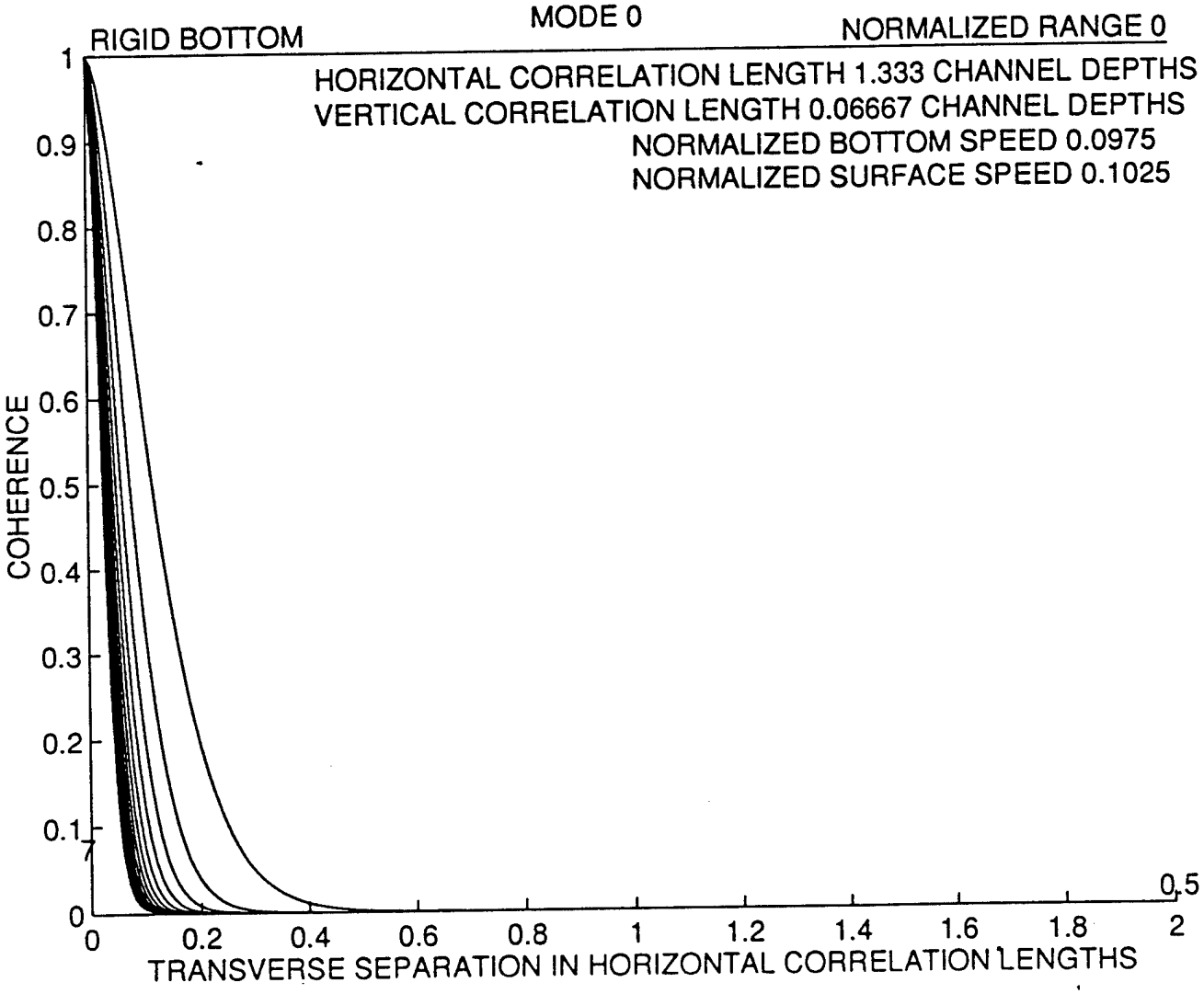

Figure 22. Mode 0 Coherence
as a Function of Transverse Separation and Range for a Rigid Bottom,
a Normalized Bottom Speed of 0.0975,
and a Normalized Surface Speed of 0.1025

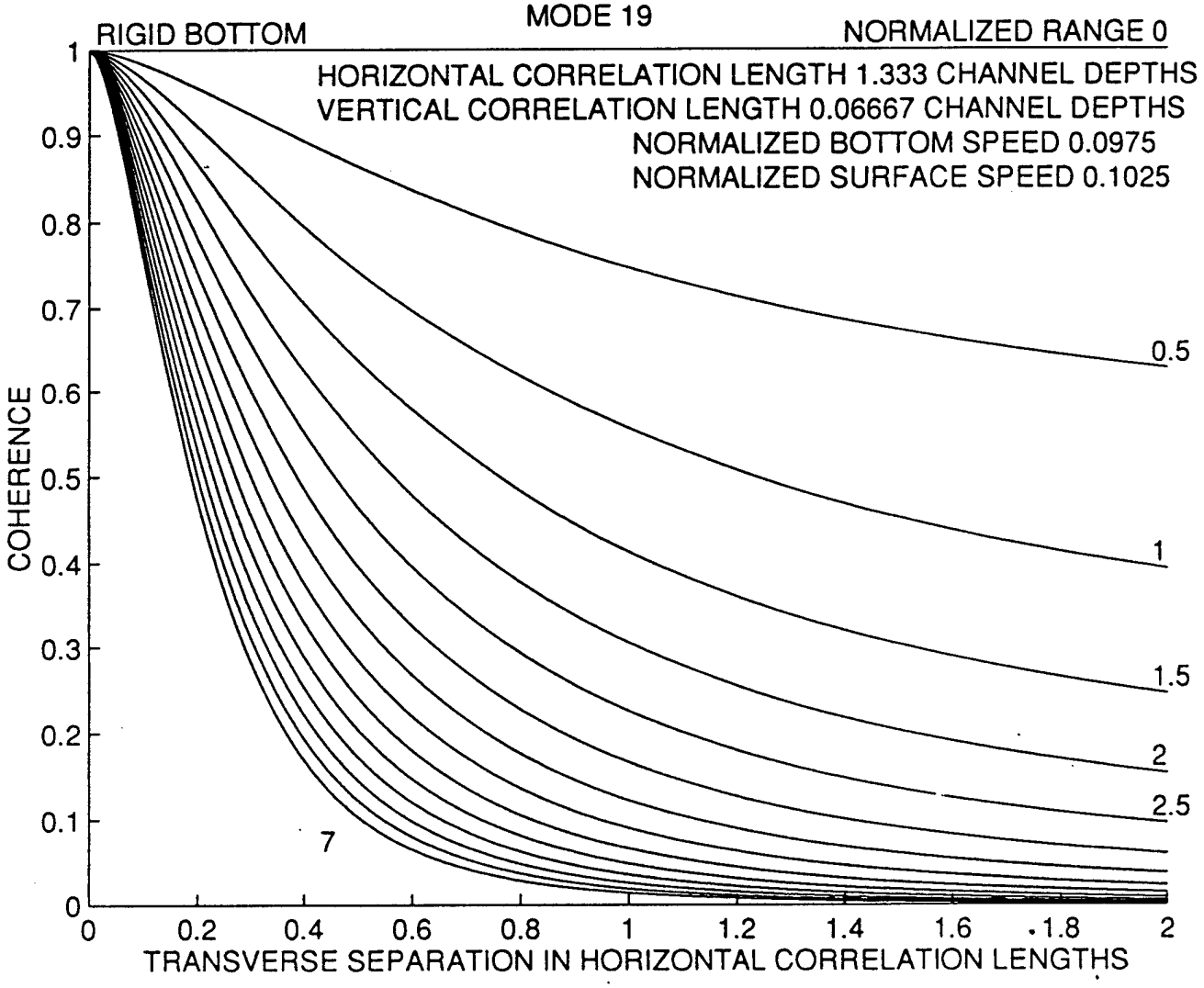

Figure 23. Mode 19 Coherence
as a Function of Transverse Separation and Range for a Rigid Bottom,
a Normalized Bottom Speed of 0.0975,
and a Normalized Surface Speed of 0.1025

modes start with equal energy flux at zero in-line propagation distance. Figure 22 shows mode 0 coherence as a function of transverse separation and in-line range. Normalized in-line range values run from 0 to 7 at increments of 0.5. Figure 23 is the corresponding set of plots for mode 19. The coherence falls off far more rapidly with range for mode 0 than for mode 19. In the coherence results of Figures 21 through 23, the shape of the horizontal refractivity fluctuation correlation function is a symmetrical exponential cusp. Accordingly, in the scattering/absorption ratio and normalized range definitions, the standard deviation σ_h is replaced by the characteristic length ℓ_h.

For comparison purposes, a constant-sound-speed case for a rigid bottom and a normalized sound speed of 0.1 completes the presentation of figures in this report. Again, the horizontal refractivity fluctuation correlation function is a symmetrical exponential cusp. Figure 24 shows the lowest and highest modes of this twenty-propagating-mode system. When all energy is initially concentrated in mode 0, Figure 25 graphs mode energy flux as a function of range for all twenty propagating modes. Eventually, each mode reaches a value of 0.05 as the range approaches infinity. When all energy is initially equally distributed among all modes, Figures 26 through 29 plot coherence as a function of transverse separation and range for modes 0, 1, 10, and 19, respectively. The coherence for mode 1 is slightly narrower than for mode 0, then steadily broadens until mode 10 is reached, and then monotonically narrows until mode 19, the narrowest, is reached. This result is completely different from the linear-sound-speed-profile results presented in Figures 23 and 24, where mode 0 (with exponential falloff as the distance from the bottom increases) has the narrowest coherence function and mode 19 (essentially a sinusoid of the highest spatial frequency) has the broadest coherence function.

When the sound speed profile is *piecewise* linear rather than simply linear, the eigenvalues can be found by starting with the zero-pressure boundary condition at the surface. Then the vertical mode wave function is determined except for the horizontal wavenumber β. Using a specific value for the wavenumber permits the vertical mode wave function to be extended down to the bottom by matching the function and its first derivative at the boundary levels where the sound speed gradient

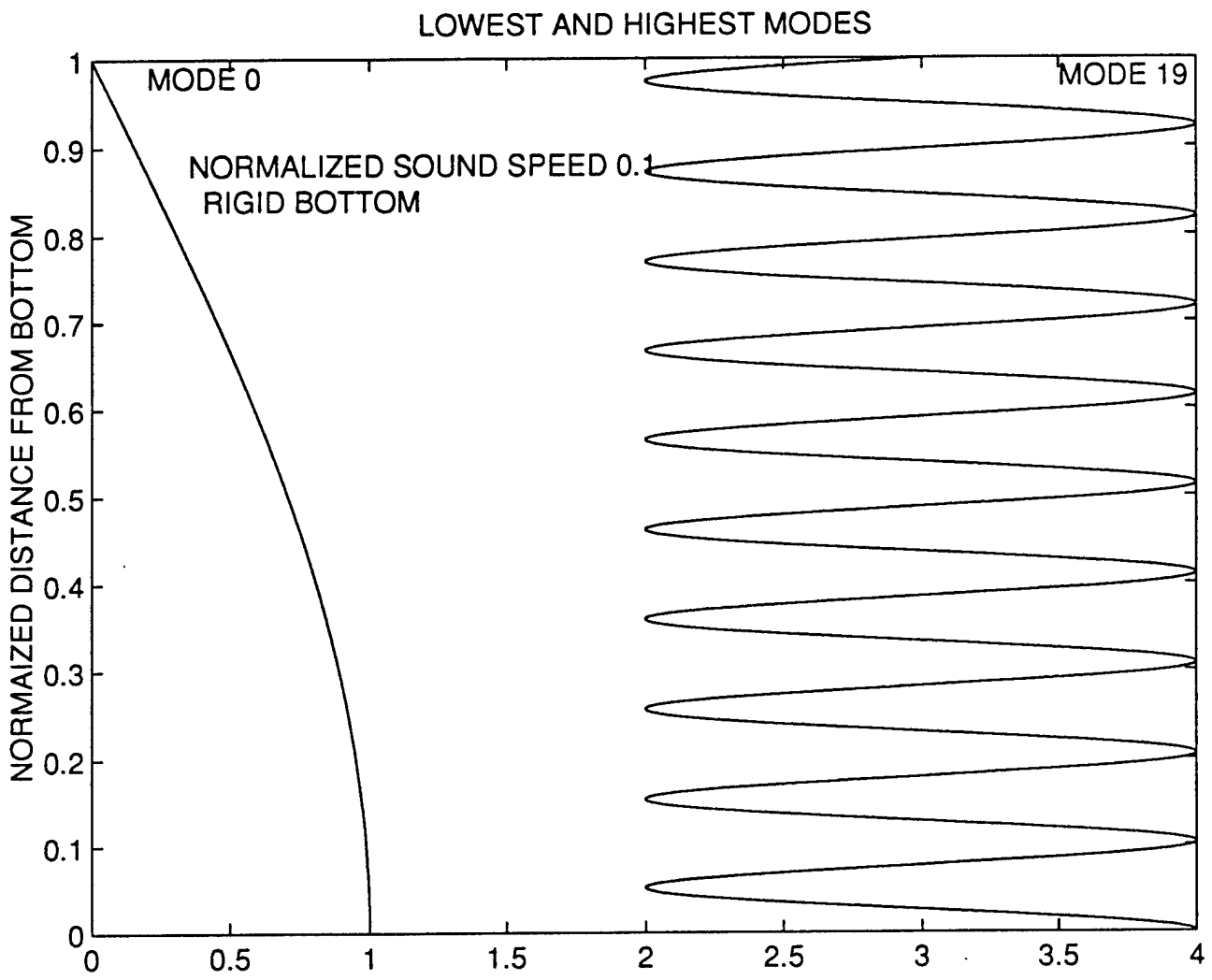

Figure 24. Lowest and Highest Modes for a Rigid Bottom and a Normalized Sound Speed of 0.1

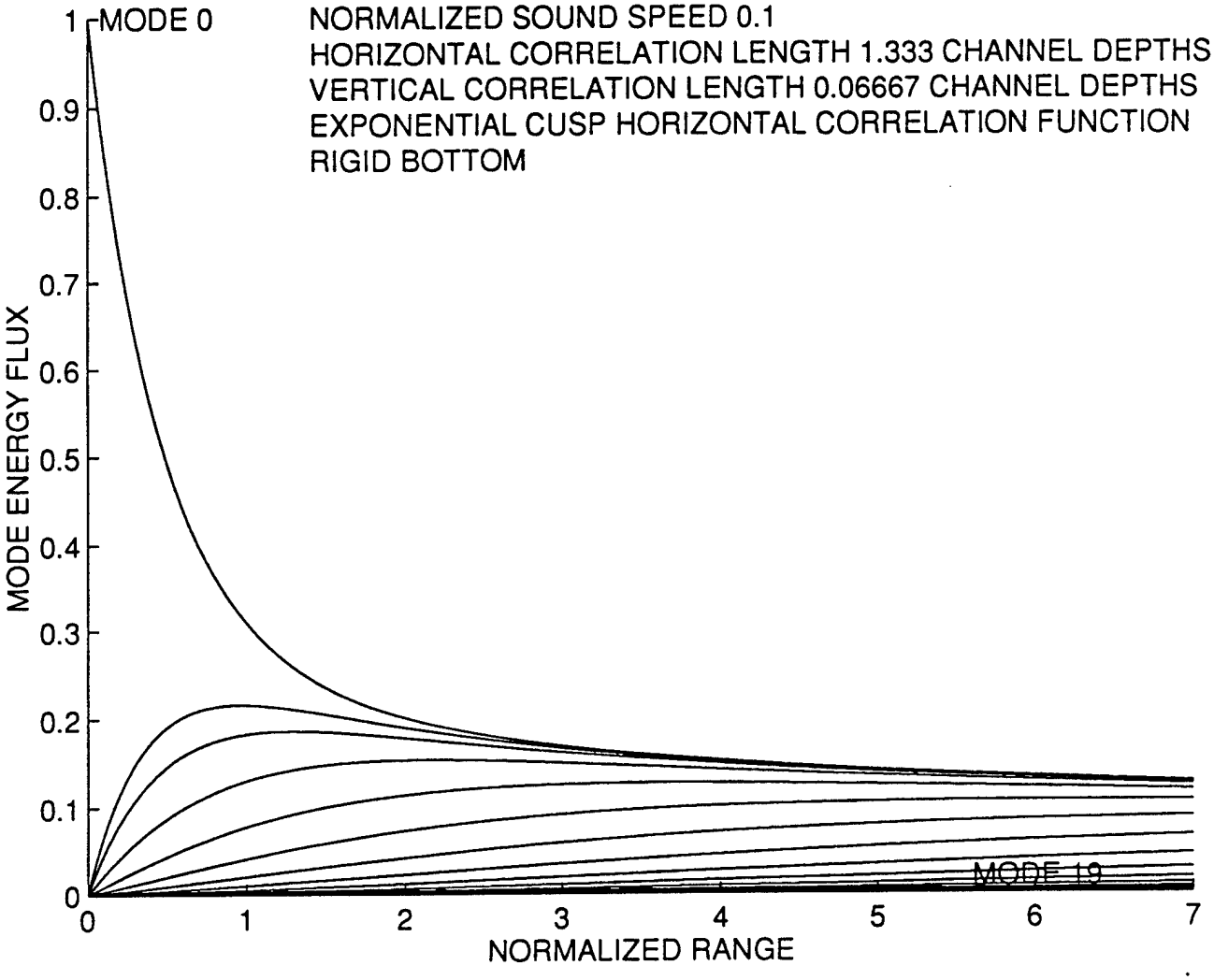

Figure 25. Mode Energy Flux as a Function of Range for a Rigid Bottom and a Normalized Sound Speed of 0.1 with Energy Initially Concentrated in Mode 0

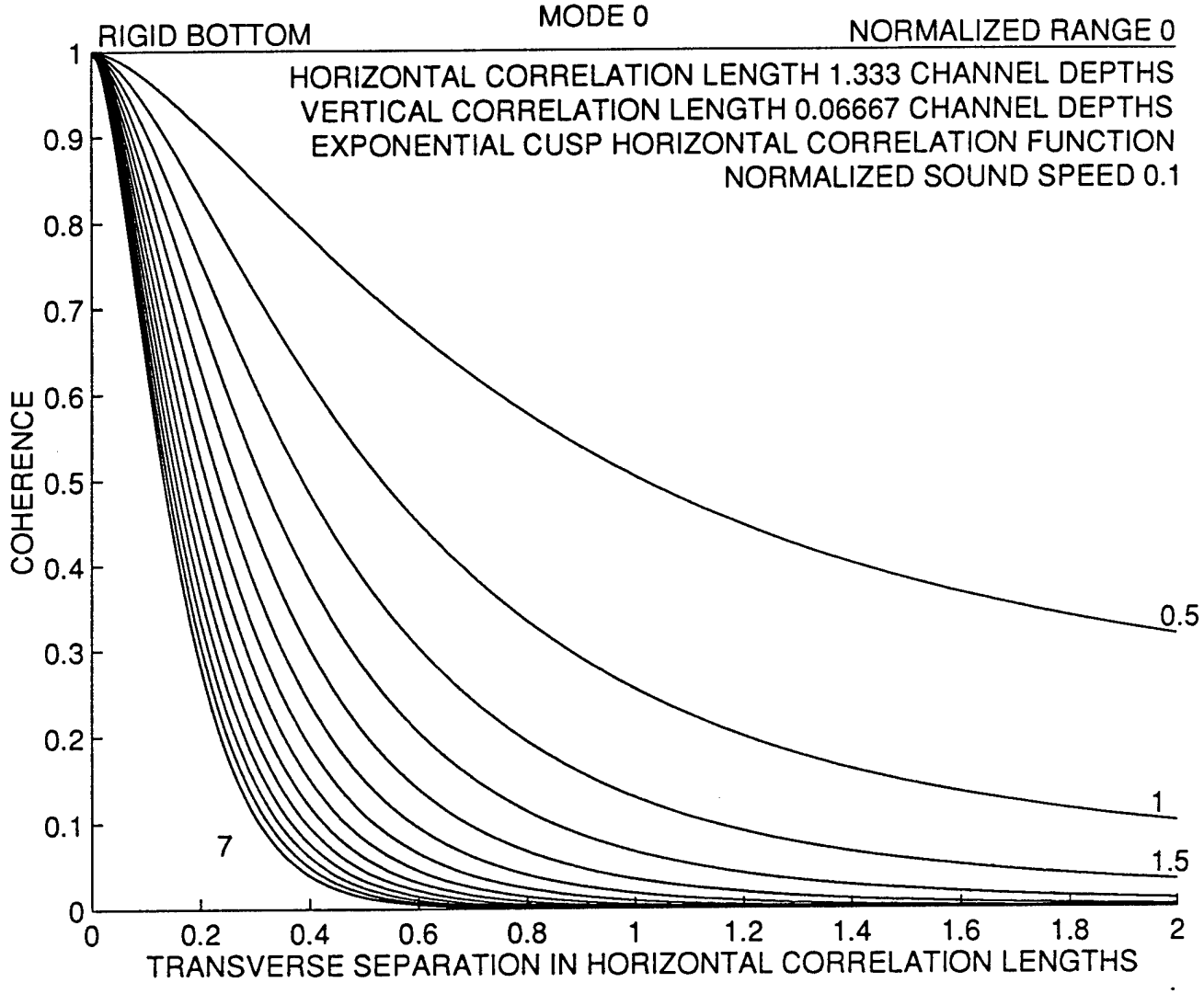

Figure 26. Mode 0 Coherence
as a Function of Transverse Separation and Range
for a Rigid Bottom and a Normalized Sound Speed of 0.1

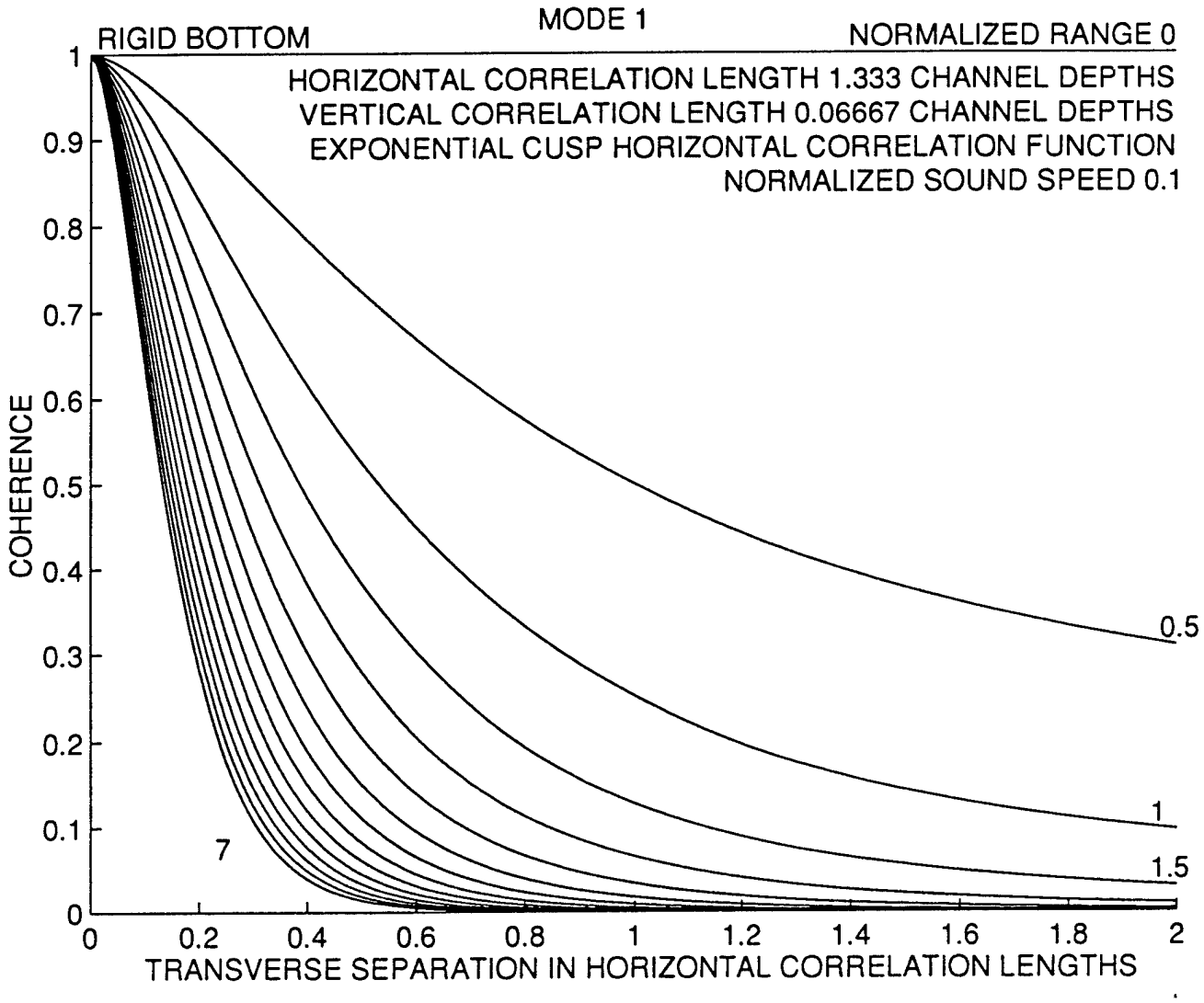

Figure 27. Mode 1 Coherence
as a Function of Transverse Separation and Range
for a Rigid Bottom and a Normalized Sound Speed of 0.1

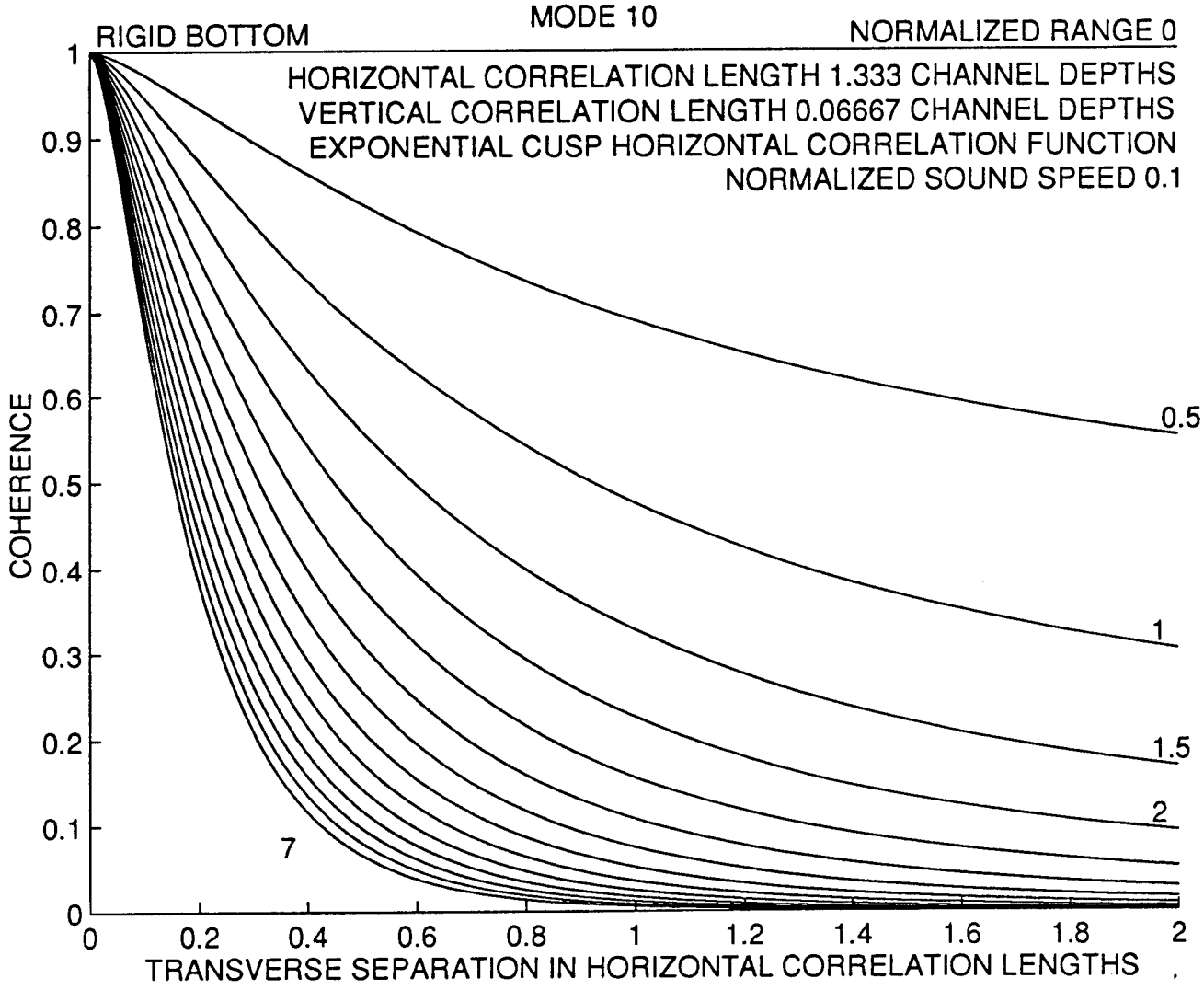

Figure 28. Mode 10 Coherence
as a Function of Transverse Separation and Range
for a Rigid Bottom and a Normalized Sound Speed of 0.1

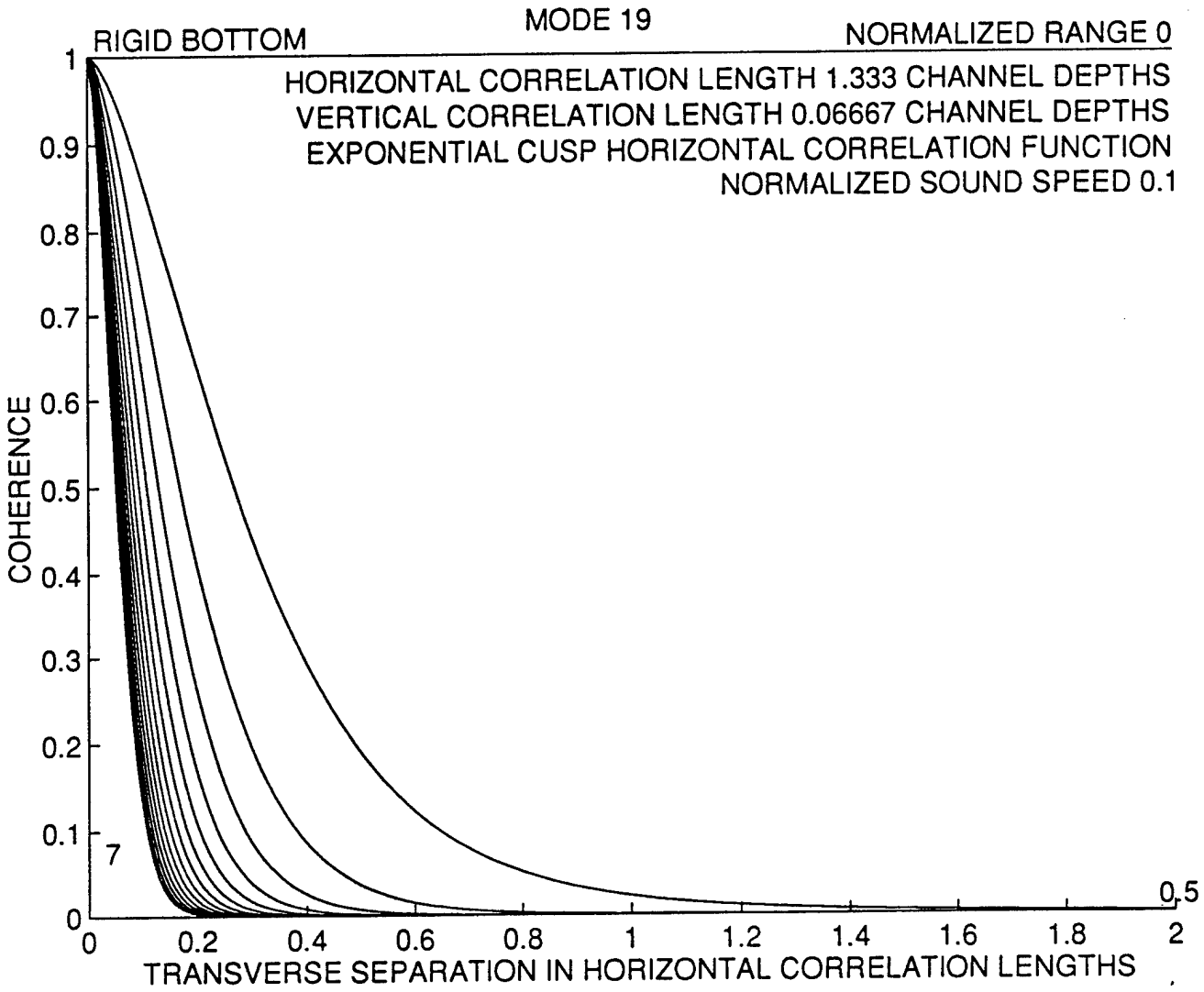

Figure 29. Mode 19 Coherence
as a Function of Transverse Separation and Range
for a Rigid Bottom and a Normalized Sound Speed of 0.1

changes. The method of extension is given in C. Allan Boyles, **Acoustic Waveguides, Application to Ocean Science**, John Wiley & Sons, New York, 1984, pp. 167-171, and Tolstoi and Clay, **Ocean Acoustics, Theory and Experiment in Underwater Sound**, McGraw-Hill, New York, 1966, pp. 86-87. At the bottom, the boundary condition for the bottom must be satisfied. Solutions exist only for a discrete set β_n of horizontal wavenumber values. These can be determined iteratively using methods similar to those used for the general bottom impedance condition and for the linear sound speed profile.

SUMMARY

The objectives of this AASERT grant effort were 1) to incorporate an absorptive bottom into the study of mode energy transfer and decay induced by volume scattering in a shallow channel and 2) to incorporate a piecewise linear sound speed profile into the study of mode energy transfer and decay induced by volume scattering in a shallow channel. Both objectives have been achieved. The introduction of an absorptive bottom generates an additional diffusion term in the coherence range-evolution differential equation and qualitatively changes the nature of the solution. The piecewise linear sound speed profile produces vertical mode wave equation solutions which are Bessel functions with pure imaginary order and pure imaginary argument. These Bessel functions are closely related to the Airy functions Ai and Bi, which are used in their representation. Final results of this effort will be found in Mr. Barnard's doctoral dissertation, which should appear early in 1998.